THE JOURNAL OF PHYSICAL CHEMISTRY A
A JOURNAL OF THE AMERICAN CHEMICAL SOCIETY

pubs.acs.org/JPCA

Article

Theoretical Rovibrational Spectroscopy of Magnesium Tricarbide—Multireference Character Thwarts a Full Analysis of All Isomers

Published as part of The Journal of Physical Chemistry virtual special issue "10 Years of the ACS PHYS Astrochemistry Subdivision".

Donatus A. Agbaglo, Qianyi Cheng, Ryan C. Fortenberry, John F. Stanton, and Nathan J. DeYonker*

Cite This: *J. Phys. Chem. A* 2022, 126, 4132–4146

Read Online

ACCESS | Metrics & More | Article Recommendations | Supporting Information

ABSTRACT: Magnesium tricarbide isomers are studied herein with coupled cluster theory and multireference configuration interaction to support their possible detection in astrochemical environments such as the circumstellar envelope surrounding the star IRC +10216 or in terrestrial laboratories. Magnesium-bearing species may abound in the interstellar medium (ISM), but only eight (MgNC, MgCN, HMgNC, MgC_2H, MgC_3N, MgC_4H, MgC_5N, and MgC_6H) have been directly identified thus far. Several possible isomers for the related MgC_3 system are explored in their singlet and triplet spin multiplicities. Overall, this work offers quantum chemical insight of rovibrational spectroscopic data for MgC_3 using quartic force fields (QFFs) based on the CCSD(T) and CCSD(T)-F12 levels of theory at the complete basis set (CBS) limit. Additional corrections with small basis set CCSDT(Q) and scalar relativistic effects are also included in the analysis. Salient multireference character is found in the singlet diamond electronic state, which makes a definitive assignment of the ground state challenging. Nevertheless, coupled cluster-based composite energies and multireference configuration interaction both predict that the $^1A_1$ diamond isomer is 1.6−2.2 kcal mol^{-1} lower in energy than the $^3A_1$ diamond isomer. Furthermore, highly accurate binding energies of various isomers MgC_3 are provided for comparison to photodetachment experiments. Dipole moments along with harmonic infrared intensities will guide efforts for astronomical and spectroscopic characterization.

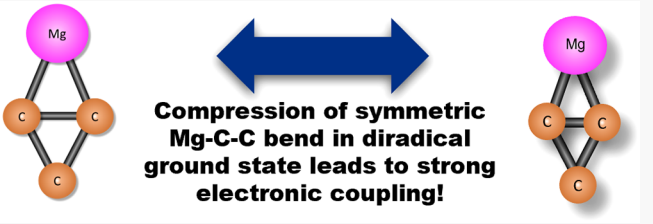

INTRODUCTION

The question of the origin of life and the habitability of other planets beyond Earth has necessitated exploration of the chemical inventory within the interstellar medium (ISM). Chemical evolution of the ISM and circumstellar regions then have indirect implications on the formation of rocky planets and exoplanets. The universal abundance of Mg is a result of stellar fusion processes in aging stars via the addition of three helium nuclei to a carbon nucleus.[1−3] Magnesium can also be produced when supernovae eject heavier-element material into the ISM. Due to the terrestrial abundance of magnesium, the element also plays a widely recognized role in materials science and in technology.[4] Astronomical identification of magnesium-bearing species began nearly two decades ago,[5−7] but confirmed detections have accelerated recently via observation of the circumstellar envelopes of aging stars, especially that of IRC +10216.

The primary mechanism for detection of molecules in the ISM and circumstellar environments has been radio astronomy supported by theoretical chemistry and laboratory spectroscopy. Our groups have focused on using quantum chemistry to provide theoretical electronic and rovibrational spectroscopy as reference data for experimental astrochemists.[8−14] A few astrochemical species bearing magnesium atoms have been detected previously in the region of the carbon-rich star IRC +10216. These include MgNC, MgCN, HMgNC, MgCCH, MgC_3N, MgC_4H, MgC_5N, and MgC_6H.[5−7,15−19] MgNC was first reported by Guélin et al. in 1986 via laboratory microwave spectroscopy, and later six transitions ranging from 107384.6 to 83538.0 MHz were observed in IRC +10216 by Guélin and Kawaguchi.[5,6] Later, MgCN, the metastable isomer of MgNC, was detected in the outer envelope of IRC +10216.[20] Observation of the $N = 11 \rightarrow 10$, $10 \rightarrow 9$, and $9 \rightarrow 8$ pure rotational transitions of MgCN were then made by Ziurys et al. again via observation of IRC +10216.[7] Closely related to the MgCN/MgNC pair is hydromagnesium isocyanide (HMgNC); and rotational lines of HMgNC ($J = 8 \rightarrow 7$, $J = 10 \rightarrow 9$, $J = 12 \rightarrow 11$, and $J = 13 \rightarrow 12$) were observed in IRC +10216, while $J = 1 \rightarrow 0$ and $J = 2 \rightarrow 1$ lines were

Received: February 24, 2022
Revised: June 9, 2022
Published: June 27, 2022

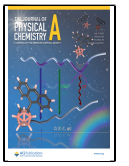

https://doi.org/10.1021/acs.jpca.2c01340
J. Phys. Chem. A 2022, 126, 4132−4146

characterized from laboratory microwave spectroscopy.[15] A theoretical study by Gronowski and Kolos[21] supported the observed rotational line assignments of HMgNC.

Subsequently, magnesium monoacetylide (MgCCH) was reported as a linear radical with a $^2\Sigma^+$ ground state by Brewster et al.,[22] and they characterized the pure rotational spectrum in the spectral range of 315−525 GHz.[22] Agúndez and coauthors observed three rotational transition doublets (N = 9 → 8 at 89.3 GHz, N = 10 → 9 at 99.3 GHz, and an obscured N = 11 → 10 line at 109.2 GHz) from IRC +10216 and tentatively assigned them to MgCCH.[17] Later, Cernicharo et al. detected additional lines confirming the observation of MgCCH in IRC +10216.[18] Other recently discovered magnesium-bearing species in IRC +10216 are of a similar construction: MgC_4H and MgC_3N. For MgC_4H and MgC_3N, Cernicharo and coauthors predicted that one set of observed lines corresponds to MgC_4H with a B_0 value of 1380.888 MHz, and a second set of observed lines corresponds to MgC_3N with a B_0 value of 1381.512 MHz.[18] MgC_3N and MgC_4H were previously investigated by quantum chemistry[23] and laboratory spectroscopy[24] which informed the analysis of observed rotational lines.[18] The most recent discovery of magnesium-containing species, the extended π-conjugated MgC_5N and MgC_6H radicals, was also in IRC +10216 from Q-band analysis in a frequency range of 31.0−50.3 GHz carried out with the 40 m Yebes Telescope in central Spain and, again, supported by quantum chemical calculations.[19]

In the chemical midst of these recently observed organometallic species, the MgC_3 molecule is a potentially fascinating molecular target since rovibrational data of MgC_3 could be used as a molecular tracer to understand the nature of the C_3 molecule in the ISM. Pure carbon chains, including C_3, are linked to the formation of circumstellar grains.[25] However, the absence of a permanent dipole moment for quasilinear and triangular isomers of C_3 prevents its detection in the ISM by submillimeter astronomy techniques.[26−28] The likely presence of C_3 in the carbon-rich star IRC +10216 has intrigued the astronomical community. Cometary ultraviolet (UV) lines at around 4050 Å are believed to originate with C_3.[26,27,29] Presently, there are no experimental spectroscopic data for MgC_3 making the quantum chemical prediction for fundamental vibrational frequencies and higher-order rovibrational properties the first point of reference for assistance in the identification of the MgC_3 ground state and confirmation of its speculated existence in any astronomical environment including IRC +10216.

In an early theoretical study, Zheng et al. predicted a fan shape (Figure 1, **5s**) as the global minimum isomer of MgC_3 with a $^1A_1$ ground electronic state.[30] They found higher energy diamond and linear isomers and did not study any isomers in the triplet spin multiplicity. Subsequently, Redondo et al. computed optimized geometries and harmonic vibrational frequencies of MgC_3 with second-order Møller−Plesset perturbation theory and density functional theory (DFT) with medium-sized basis sets (MP2/6-311G and B3LYP/6-311G). They examined seven geometry types in both singlet and triplet spin multiplicities (12 structures total, Figure 1).[31] Surprisingly, a large number of low-energy isomers reported by Redondo would be thermally accessible at room temperature. Relative energies of the lowest-lying isomers were further studied with coupled cluster theory and composite G1/G2 methods. The most reliable level of theory in this previous work, coupled cluster singles, doubles, and perturbative triples

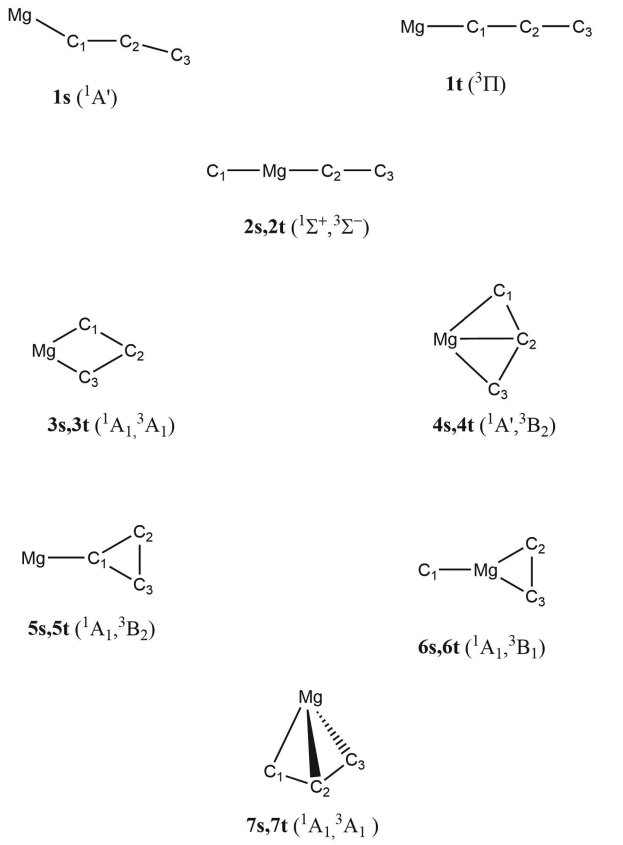

Figure 1. Schematic representation of the various isomers of MgC_3.

CCSD(T)/6-311G(2df), predicted that six of the 12 possible isomers, singlet "zigzag", triplet linear, singlet and triplet diamond, triplet kite, and triplet fan, were within 10 kcal mol^{-1} in energy. Coupled cluster results suggested the singlet and triplet diamond isomers were nearly isoenergetic. However, they showed a slight basis set dependence where the triplet state was favored with larger Pople-style basis sets. Such competition between singlet and triplet spin multiplicities is unexpected for s-block metal-containing molecules. Due to the near-degeneracy in the diamond isomer and the relatively low-level electronic structure techniques used, Redondo et al. could not conclusively establish which of the MgC_3 isomers is the ground state structure.[31]

Similar challenges in characterizing the ground state were faced in the theoretical study of SiC_3 between the linear triplet isomer and the diamond-shaped singlet isomer with Si−C transannular bonding,[32] but thereafter, laboratory analysis and interstellar medium observation showed that the diamond isomer of SiC_3 (X^1A_1) is the ground state.[33−37] This was further validated with several computational and experimental studies.[37−41]

Graham and coauthors have studied the structure and vibrational spectroscopy of MgC_3^- using Fourier transform infrared (FTIR) spectroscopy and DFT. Four isomers of MgC_3^- were predicted to be low-lying, and the linear isomer ($^4\Sigma$) was computed to be the lowest-energy isomer with a nonlinear doublet isomer only ∼3 kcal mol^{-1} higher in energy.[42] FTIR-derived vibrational analysis from Graham corroborates the linear quartet as the observed MgC_3^- structure. Now that post-CCSD(T) calculations and correlated multireference techniques are more mainstream, a higher-level

https://doi.org/10.1021/acs.jpca.2c01340
J. Phys. Chem. A 2022, 126, 4132−4146

treatment of neutral MgC_3 rovibrational spectroscopy is prudent.

To probe the ISM for the presence of MgC_3 through the use of modern astronomical telescopes such as the Atacama Large Millimeter/Submillimeter Array (ALMA) and other well-known radio telescopes such as the IRAM 30-m and Yebes 40-m radio telescopes, highly accurate computational or terrestrial gas phase data is necessary for comparison to observations. In this work, a quantum chemical study of magnesium tricarbide (MgC_3) is presented in order to establish more firmly its ground state isomer and to aid in its possible detection in the laboratory or even in IRC +10216 and beyond. Composite methods based on coupled cluster theory[43] [CCSD(T)] and with explicit correlation are employed [CCSD(T)-F12].[44,45] Additionally, coupled cluster is pushed beyond the CCSD(T) "gold standard" in tandem with multireference configuration interaction (MRCI) techniques to confirm the ground state identity.

COMPUTATIONAL DETAILS

Preliminary calculations of MgC_3 used DFT (B3LYP/6-31G*)[46] and second-order Møller−Plesset perturbation theory[47] (MP2/cc-pVTZ) to qualitatively explore isomeric and conformational energy differences. These results are utilized for initial screening of the optimized isomers and labeled with the same convention as in the previous study by Redondo et al. The Gaussian16 program is utilized in the initial calculations.[48−50] With the aim of getting more refined spectroscopic data that would better assist in the astronomical detection of MgC_3, coupled cluster theory[43] both via conventional CCSD(T) and with explicit correlation [CCSD(T)-F12b][44,45] is utilized to construct a composite approach to compute relative energies of isomers and quartic force fields (QFFs). Explicitly correlated methods have recently been shown to produce notably accurate results for QFF calculations of organic molecules.[51−55]

Optimized geometries are computed for all low-lying states of MgC_3 from CCSD(T) calculations based on the spin-restricted Hartree−Fock (RHF/ROHF)[56,57] reference wave functions with a series of correlation consistent basis sets.[58,59] All open-shell coupled cluster computations in MOLPRO are carried out with the partially spin-adapted "R/UCC" formalism.[60] Some computations make use of the second-order Douglas-Kroll (DK) Hamiltonian[61] with correlation consistent basis sets optimized for DK energies. The core correlation effects are examined using weighted core−valence correlation consistent basis sets,[59] which are specifically designed to treat core correlation by unfreezing the 1s carbon orbitals and 2s/2p orbitals of magnesium. The 1s orbital of the Mg center remains frozen in order to adhere to the basis set design. The three levels of theory and the basis sets that define the reference QFF geometry are valence CCSD(T)-F12/cc-pVQZ (VQZ-F12), valence cc-pCVTZ-F12 (CVTZ-F12), and core−valence cc-pCVTZ-F12 (1 core CVTZ-F12). In all cases, geometric parameters for the composite values are obtained by

$$s_{\text{QFF reference}} = s_{\text{VQZ-F12}} + (s_{\text{1 core CVTZ-F12}} - s_{\text{valence CVTZ-F12}}) \quad (1)$$

where s in the above equation defines the value of a general internal coordinate of the composite optimized geometries.

The necessary vibrational frequencies and rotational constants have been computed for the various isomers via quartic force field (QFF) computations, fit to a fourth-order Taylor series expansion of the internuclear Hamiltonian in the form

$$V = \frac{1}{2}\sum_{ij} F_{ij}\Delta_i\Delta_j + \frac{1}{6}\sum_{ijk} F_{ijk}\Delta_i\Delta_j\Delta_k + \frac{1}{24}\sum_{ijkl} F_{ijkl}\Delta_i\Delta_j\Delta_k\Delta_l \quad (2)$$

where Δ_i are displacements of internal coordinate s for the given index (i), and $F_{ij...}$ are the force constants of the same unrestricted indices.[62] QFF calculations for displacements up to fourth-order are made in increments of 0.005 Å for bond lengths or 0.005 radians for the bond angles, torsion angles, and pseudolinear bends. Internal or symmetry-adapted internal coordinate definitions and the relationship of internal coordinates to computed normal modes of vibration for all isomers are defined in the Supporting Information. Note that reported theoretical r_0 values throughout are more appropriately described as zero-point vibrationally averaged r_α bond distances.

Several levels of theory are required to compute the complete basis set extrapolation "C" in addition to consideration of core−valence electron correlation "cC" and a scalar relativistic correction "R".[63−67] For each point, CCSD(T) energies with aug-cc-pVQZ and aug-cc-pV5Z basis sets are extrapolated to the complete basis set (CBS) limit with a two-point formula.[68−70]

$$E(l) = E(\text{CBS}) + A\left(l_{\max} + \frac{1}{2}\right)^{-4} \quad (3)$$

The composite energy (CcC) of each single point is defined as

$$E(\text{CcC}) = E_{\text{CBS/aV}\infty\text{Z}} + (E_{\text{1 core/wCVQZ}} - E_{\text{valence/wCVQZ}}) \quad (4)$$

With a Douglas-Kroll correction δ(DK) applied to the CcC surface, the CcCR composite QFF is obtained with the following equation:

$$\delta(\text{DK}) = E[\text{aug-cc-pVTZ-DK/CCSD(T)}] - E[\text{aug-cc-pVTZ/CCSD(T)}] \quad (5)$$

A CcC-F12 approach is employed using CCSD(T)-F12b energies similar to the CcC composite method (CcCR). The CcC-F12 approach is defined with the following expression:

$$E(\text{CcC-F12}) = E_{\text{VQZ-F12}} + (E_{\text{1 core/CVTZ-F12}} - E_{\text{valence/CVTZ-F12}}) \quad (6)$$

The δ(DK) corrections from conventional coupled cluster computations are added to the CcC-F12 data to obtain CcCR-F12 spectroscopic constants.

An additional energy correction for "post-CCSD(T)" electron correlation is performed using single point CCSDT(Q)/aug-cc-pVDZ computations at the CCSD(T)/aug-cc-pVDZ optimized geometry.

$$\delta[\text{CCSDT(Q)}] = E[\text{aug-cc-pVDZ/CCSDT(Q)}] - E[\text{aug-cc-pVDZ/CCSD(T)}] \quad (7)$$

To support reproducibility of the QFF calculations, the reader should note that the aug-cc-pVDZ CCSD(T) force fields are computed from the aug-cc-pVDZ CCSD(T) optimized geometries rather than the composite geometries obtained via eq 1. When dealing with metal-containing systems, we are accumulating evidence of numerical issues when the CcC reference geometry is too far from the

https://doi.org/10.1021/acs.jpca.2c01340
J. Phys. Chem. A 2022, 126, 4132−4146

Table 1. Electronic Configuration of MgC_3 Isomers with the aV5Z-DK CCSD(T) Level of Theory

electronic state		electronic configuration	T_1	D_1	$\|t_{1max}\|$	$\|t_{2max}\|$
diamond **3s**	$^1A_1$	[core] $(6a_1)^2$ $(3b_2)^2$ $(7a_1)^2$ $(2b_1)^2$ $(8a_1)^2$ $(4b_2)^2$ $(9a_1)^2$	0.034	0.108	0.068	0.303
diamond **3t**	$^3A_1$	[core] $(6a_1)^2$ $(3b_2)^2$ $(7a_1)^2$ $(2b_1)^2$ $(8a_1)^2$ $(4b_2)^2$ $(9a_1)^1$ $(10a_1)^1$	0.028	0.086	0.121	<0.050
linear **1t**	$^3\Pi$	[core] $(7\sigma)^2$ $(8\sigma)^2$ $(9\sigma)^2$ $(2\pi)^4$ $(10\sigma)^2$ $(11\sigma)^1$ $(3\pi)^1$	0.037	0.105	0.148	0.055
zigzag **1s**	$^1A'$	[core] $(8a')^2$ $(9a')^2$ $(10a')^2$ $(11a')^2$ $(12a')^2$ $(2a'')^2$ $(13a')^2$	0.054	0.188	0.160	0.324
kite **4s**	$^1A_1$	[core] $(6a_1)^2$ $(3b_2)^2$ $(7a_1)^2$ $(8a_1)^2$ $(2b_1)^2$ $(4b_2)^2$ $(5b_2)^2$	0.025	0.057	<0.050	<0.050
kite **4t**	$^3B_2$	[core] $(6a_1)^2$ $(3b_2)^2$ $(7a_1)^2$ $(8a_1)^2$ $(2b_1)^2(4b_2)^2$ $(5b_2)^1(1a_2)^1$	0.025	0.054	0.071	0.072
fan **5s**	$^1A_1$	[core] $(6a_1)^2$ $(3b_2)^2$ $(7a_1)^2$ $(8a_1)^2$ $(2b_1)^2$ $(4b_2)^2$ $(9a_1)^2$	0.024	0.057	<0.050	0.256
fan **5t**	$^3B_2$	[core] $(6a_1)^2$ $(3b_2)^2$ $(7a_1)^2$ $(8a_1)^2$ $(2b_1)^2$ $(9a_1)^2$ $(4b_2)^1$ $(10a_1)^1$	0.023	0.064	0.082	<0.050

equilibrium position of the small basis set CCSD(T)/CCSDT/CCSDT(Q) surface. The primary cause of the numerical issues is that core-valence correlation has a more substantial effect on inorganic molecules than it does on organic molecules. Thus, the minimum of valence force fields may lie completely outside of the computed energy grid, which erodes the ability to fit a polynomial function for the QFF.

The least-squares fit of the QFF energy surface identifies the minimum QFF equilibrium geometry. The residual sum of squares reported for the **3t** and **1s** isomers are lower than 10^{-16} $(au)^2$, while the fits are worse for the **1t** [10^{-12} $(au)^2$] and **3s** isomers [10^{-10} $(au)^2$], see below. All geometry optimizations and CCSD(T) energy point computations are performed with the MOLPRO 2019.1 program.[57] Post-CCSD(T) computations are calculated using the MRCC[71] software package, which is a string-based program for arbitrary-order coupled cluster theory. Energy computations with MRCC use one-/two-electronic integrals and reference wave functions generated by the MOLPRO 2019.1 software package.[57,72−79] The derivative information is then input into the INTDER package[80] for the transformation of the force constants from symmetry-internal to Cartesian coordinates. The anharmonic frequencies and the CcCR and CcCR-F12 spectroscopic constants are computed with the SPECTRO[81] program via second-order rotational and vibrational perturbation theory (VPT2).[82] The $^3A_1$ diamond isomer presents a need for polyad resonance inclusion because the vibrational states have multiple resonance couplings. Each state has a unique polyad quantum number which is employed in labeling both the zero-order wave function and anharmonic states.[83] The importance of this concept was first put forward by Dubal and Quack.[84]

The dipole moment is computed at the center of mass for the optimized geometry at a given level of theory, and the double-harmonic vibrational intensities are computed using MP2/aug-cc-pVDZ in Gaussian16, which has been shown to produce good agreement with higher-level theory for semi-quantitative interpretation of the vibrational intensities.[85,86]

Additional multireference configuration interaction energies and optimized geometries are computed using the internally contracted singles and doubles scheme in MOLPRO with the Davidson correction (MRCISD+Q).[87−89] Complete active space self-consistent field (CASSCF) computations are first used to create the set of reference configuration state functions (CSFs) using an active space of 10 electrons/11 MOs. All CSFs are used in the subsequent MRCISD+Q computation, performed with cc-pVTZ-DK basis sets and incorporating the DK Hamiltonian throughout.

RESULTS AND DISCUSSION

From the preliminary B3LYP and MP2 computations, a few isomers of MgC_3 are ruled out for further discussion. In agreement with the computations of Redondo et al., the singlet linear MgC_3 state, both the singlet and triplet linear $CMgC_2$ isomers (**2s, 2t**), and fan-shaped $CMgC_2$ structures (**6s, 6t**) as shown in Figure 1 are all at least 50 kcal mol^{-1} higher in energy compared to the diamond-shaped isomers at the B3LYP/6-31G(d), MP2/cc-pVTZ, and CCSD(T)/aug-cc-pVDZ levels of theory. Pyramidal isomers (**7s, 7t**) not previously explored by Redondo et al. are also found to be higher than 50 kcal mol^{-1} in energy compared to the diamond-shaped isomers. Structural, energetic, and harmonic vibrational properties are reported for eight isomers: singlet zigzag (**1s**), linear triplet (**1t**), singlet and triplet diamond (**3s, 3t**), singlet and triplet kite (**4s, 4t**), and singlet and triplet fan (**5s, 5t**).

Electronic Structure. The electronic configurations of the eight lowest-energy isomers and their orbital occupations are variationally accessible with single-reference methods and have been examined with coupled cluster theory. Detailed electronic configurations of the eight lowest-energy isomers are given in Table 1.

Electronic excitation from the singlet diamond isomer **3s** to the triplet diamond isomer **3t** involves a spin-flip via the $9a_1 \rightarrow 10a_1$ transition. The $9a_1$ MO of the **3s** isomer is mostly Mg 3s character (see the contour plot in Figure S1) with mixing of 2s and $2p_z$ lone pair character from the vertex carbon atoms. The $10a_1$ MO of the **3s** isomer (Figure S2), which has significant fractional occupation in CASSCF/MRCISD+Q calculations, is mixed among all four atoms. While the $10a_1$ MO shows some amount of bonding between $2p_z$ orbitals of the C atoms in the middle of the diamond, there is more pronounced antibonding between the C atoms and Mg. Interestingly, in the triplet diamond isomer **3t**, the $10a_1$ singly occupied MO has entirely Mg $3s/2p_z$ character, while the $9a_1$ singly occupied MO has no density on the Mg center and exhibits σ-antibonding and weak π-bonding between the two carbon atoms closer to the Mg atom (see Figure S3). Apparent destabilization of the Mg 3s orbital is the first sign of multireference character in the MgC_3 system. While the singlet fan isomer **5s** has the same electronic configuration as the diamond **3s** state, the triplet fan **5t** state arises from a $4b_2 \rightarrow 10a_1$ transition.

From Table 1, rather surprising manifestations of multireference character are evident in the singlet isomers. T_1 diagnostics for all computed isomers (ranging from 0.023 to 0.054) in both singlet or triplet spin multiplicities are small and mostly within the acceptable tolerance of 0.05.[42] However, multireference character of metal-containing molecules must be holistically assessed.[90,91] The D_1 diagnostic values are larger for most isomers but do not provide compelling evidence of

https://doi.org/10.1021/acs.jpca.2c01340
J. Phys. Chem. A 2022, 126, 4132−4146

Table 2. Relative Energies (kcal mol^{-1}) of the MgC_3 Species at Different Levels of Theory

this work	diamond ($^3A_1$) **3t**	diamond ($^1A_1$) **3s**	linear ($^3\Pi$) **1t**	zigzag ($^1A'$) **1s**	kite ($^3B_1$) **4t**	fan ($^3B_1$) **5t**	fan ($^1A_1$) **5s**	kite ($^1A_1$) **4s**	linear ($^1\Sigma$)
CCSD(T)/aug-cc-pVTZ	0.3	0.0	1.6	2.4	5.7	9.7	16.5	27.6	39.9
CCSD(T)/aug-cc-pVQZ	0.0	0.1	2.1	3.0	6.3	9.6	16.8	27.1	40.0
CCSD(T)/aug-cc-pV5Z	0.0	0.2	2.5	3.5	6.7	9.7	17.1	26.6	39.8
CCSD(T)/aug-cc-pVDZ-DK	1.7	0.0	2.0	1.6	5.7	10.5	15.5	31.7	41.9
CCSD(T)/aug-cc-pVTZ-DK	0.4	0.0	1.6	2.3	5.7	9.7	16.4	27.8	40.0
CCSD(T)/aug-cc-pVQZ-DK	0.0	0.0	2.1	2.9	6.3	9.6	16.7	27.2	40.0
CCSD(T)/aug-cc-pV5Z-DK	0.0	0.1	2.5	3.4	6.6	9.6	16.9	26.7	39.9
CCSD(T)/aug-cc-pV(D+d)Z	1.5	0.0	2.1	1.9	5.8	10.6	15.9	30.1	41.0
CCSD(T)/aug-cc-pV(T+d)Z	0.2	0.0	1.6	2.4	5.8	9.8	16.6	26.9	39.3
CCSD(T)/aug-cc-pV(Q+d)Z	0.0	0.1	2.2	3.1	6.4	9.6	16.9	26.6	39.5
CCSD(T)/aug-cc-pV(5+d)Z	0.0	0.2	2.6	3.5	6.7	9.7	17.1	26.6	39.7
CCSD(T)/valence cc-pwCVQZ	0.0	0.2	2.3	3.3	6.4	9.8	16.9	26.7	40.0
CCSD(T)/cc-pwCVQZ	0.0	0.3	2.3	3.8	6.5	9.7	17.1	27.4	40.4
CCSD(T)/valence aug-cc-pwCVQZ	0.0	0.1	2.2	3.2	6.4	9.6	16.9	26.5	39.5
CCSD(T)/aug-cc-pwCVQZ	0.0	0.4	2.3	3.7	6.6	9.6	17.0	27.0	39.9
CCSD(T)/valence aug-cc-pwCVQZ-DK	0.0	0.0	2.2	3.1	6.4	9.6	16.8	26.6	39.5
CCSD(T)/aug-cc-pwCVQZ-DK	0.0	0.2	2.2	3.6	6.5	9.5	16.8	27.1	39.9
CCSD(T)-F12/cc-pVDZ-F12	0.2	0.0	3.2	3.7	7.2	9.7	17.0	27.9	41.0
CCSD(T)-F12/cc-pVTZ-F12	0.0	0.1	2.8	3.7	6.9	9.7	17.1	26.8	40.2
CCSD(T)-F12/cc-pVQZ-F12	0.0	0.2	2.8	3.7	6.9	9.7	17.2	26.5	39.9
CCSD(T)-F12/valence-cc-pwCVTZ-F12	0.0	0.2	2.8	3.7	6.9	9.7	17.1	26.7	40.1
CCSD(T)-F12/cc-pwCVTZ-F12	0.0	0.4	2.8	4.2	7.0	9.6	17.1	27.1	40.4
CCSDT(Q)/aug-cc-pVDZ	3.5	0.0	3.0	2.2	7.0	12.2	16.0		
CcC	0.0	0.4	2.9	4.4	7.1	9.6	17.3		
CcC-F12	0.0	0.5	2.7	4.2	7.0	9.6	17.2		
CcCR	0.0	0.3	2.8	4.3	7.1	9.6	17.1		
CcCR-F12	0.0	0.4	2.7	4.0	7.0	9.5	17.0		
CcC + δ[CCSDT(Q)]	1.5	0.0	3.5	4.5	8.0	11.0	17.2		
CcCR + δ[CCSDT(Q)]	1.5	0.0	3.4	4.5	8.0	11.0	17.2		
Previous studies									
MP2(full)/G-311G(d)[a]	0.0	3.9	21.0	14.1	15.3	10.0	19.2	36.5	
B3LYP/6-311G(d)[a]	3.4	10.2	0.0	5.1	6.9	8.3	18.9	34.2	
CCSD(T)/6-311G(d)+G(d)[a]	0.9	0.0	1.6	1.6	5.2	7.0	14.6	32.2	
CCSD(T)/6-311G(2df)[a]	0.0	0.3	1.8	2.8	4.7	7.5	16.9	28.9	

[a]Previous results from ref 31.

multireference character and range from 0.054−0.188. Singlet isomers show larger D_1 diagnostic values than their triplet counterparts. When the largest t_1/t_2 amplitudes of each isomer are carefully analyzed, salient multireference character is finally revealed. The **1s**, **1t**, and **3t** isomers have $|t_{1max}|$ values greater than 0.100, suggesting post-CCSD(T) electron correlation may be important. Furthermore, the very large maximum t_2 amplitudes of the singlet isomers (**1s**, **3s**, and **5s**) are indicators that the reliability of coupled cluster calculations may be compromised. Particularly, the singlet diamond (**3s**) maximum t_2 amplitude of 0.303 between the HOMO and LUMO suggests that there is a significant amount of biradical character (comparable to the ozone case study) in the overall wave function. Indeed, the MRCISD C_0 coefficient for the **3s** isomer is only 0.75, while the absolute value of C_1 is 0.51! MRCISD calculations are shown likely to be necessary in order to correctly identify the ground state of MgC_3.

Relative Electronic Energies and the Ground Electronic State. Relative electronic energies of the eight lowest-lying isomers with coupled cluster theory [CCSD(T) and CCSD(T)-F12] and various correlation consistent basis sets are displayed in Table 2. Interestingly, the basis set dependence of the relative energies is weak on the absolute scale, with observed changes of less than 2 kcal mol^{-1}. However, these differences become extremely important when comparing the isomers within 4.5 kcal mol^{-1} of the ground state. Small basis sets favor the singlet diamond isomer **3s**, which is 1.7 kcal mol^{-1} lower in energy than **3t** at the CCSD(T)/aug-cc-pVDZ-DK level of theory. Moving to a QZ-sized basis set, the singlet and triplet diamond isomers are nearly isoenergetic, within 0.1 kcal mol^{-1} in energy. At the CCSD(T)/aug-cc-pV(5+d)Z level of theory, the **3t** isomer is now favored by 0.2 kcal mol^{-1}. The inclusion of scalar relativity via the DK Hamiltonian slightly favors the **3s** isomer as the ground state. Overall, scalar relativity has a small influence on the electronic structure and energetics of MgC_3, which is expected. Outer core electron correlation pushes relative energies in favor of **3t** by ∼0.2 kcal mol^{-1}. Large basis set conventional CCSD(T) relative energies are in agreement with large basis set CCSD(T)-F12b relative energies to within 0.2 kcal mol^{-1} for most higher-energy isomers except the triplet linear (**2t**) isomer. Larger basis sets also slightly increase the

https://doi.org/10.1021/acs.jpca.2c01340
J. Phys. Chem. A 2022, 126, 4132−4146

relative energies of linear, zigzag, kite, and fan isomers compared to the diamond isomers. Composite relative energies (CcC, CcC-F12, CcCR, and CcCR-F12) are consistent to within 0.2 kcal mol^{-1}. The final CcCR isomeric relative energies are as follows (in kcal mol^{-1}): 0.0 (**3t**) < 0.3 (**3s**) < 2.8 (**1t**) < 4.3 (**1s**) < 7.1 (**4s**) < 9.6 (**6t**) < 17.1 (**6s**). Finally, the effect of δ[CCSDT(Q)] on relative energies is also shown in Table 2. Except for the two diamond isomers, higher-order coupled cluster theory does not qualitatively change relative isomeric energies and does not change the energy ordering of states. However, δ[CCSDT(Q)] does crucially seem to change the identity of the MgC_3 ground state.

A detailed comparison of higher-order coupled cluster and MRCISD+Q results for the **3s** and **3t** isomers is shown in Table 3. Surprisingly, post-CCSD(T) relative energies are as

Table 3. Relative Energy (kcal mol^{-1}) between Diamond ($^3A_1$) 3t and Diamond ($^1A_1$) 3s Isomers

	diamond ($^3A_1$) **3t**	diamond ($^1A_1$) **3s**
CCSD(T)/aug-cc-pVDZ	1.5	0.0
CCSD(T)/aug-cc-pVTZ	0.3	0.0
CcC	0.0	0.4
CcCR	0.0	0.3
CCSDT/aug-cc-pVDZ	0.9	0.0
CCSDT/aug-cc-pVTZ	0.0	0.5
Δ[CCSDT-CCSD(T)]		+0.8
CcCR + CCSDT	0.0	1.1
CCSDT(Q)/aug-cc-pVDZ	3.5	0.0
CCSDT(Q)/aug-cc-pVTZ	2.8	0.0
Δ[CCSDT(Q)-CCSDT]		−3.3
CcCR + CCSDT(Q)	2.2	0.0
CcCR + CCSDT(Q) + ΔZPVE	2.5	0.0
MRCISD+Q/cc-pVTZ-DK	1.9	0.0
MRCISD+Q/cc-pVTZ-DK + ΔZPVE	2.2	0.0

basis set dependent as the CCSD(T) relative energies. CCSDT/aug-cc-pVDZ single point energies [run at the CCSD(T)/aug-cc-pVDZ optimized geometry] stabilize the **3s** state by 0.6 kcal mol^{-1}. However, performing CCSDT/aug-cc-pVTZ single point energies [similarly run at the CCSD(T)/aug-cc-pVDZ optimized geometry] shifts the relative energy 1.4 kcal mol^{-1} in favor of the **3s** isomer. The effect of full triples on a Mg-containing molecule seems unusually significant, with CcCR + δ[CCSDT] using TZ basis sets predicting a **3s** ground state isomer by 1.1 kcal mol^{-1}. The subsequent effect of CCSDT(Q)/aug-cc-pVDZ single point computations is relatively massive; the relative energies of the diamond isomers are shifted 2.0 kcal mol^{-1} in favor of the **3s** isomer. Again, using a larger basis set with CCSDT(Q) favors the **3t** isomer, but the difference is too great to overcome. The correction for CCSDT(Q)/aug-cc-pVTZ - CCSDT/aug-cc-pVTZ shifts relative energies 3.3 kcal mol^{-1} toward the singlet isomer. With the CcCR composite method corrected for δ[CCSDT(Q)], the **3s** isomer is 1.6 kcal mol^{-1} lower in energy than the **3t** state. With reasonable confidence, the singlet−triplet gap should be qualitatively converged with respect to the basis set and electron correlation effects, and a $^1A_1$ diamond ground electronic state is assigned here to the MgC_3 molecule. This assignment is validated by multireference results shown in Table 3. The highly multireference $^1A_1$ diamond isomer (**3s**) is computed to be 1.9 kcal mol^{-1} lower in energy than the $^3A_1$ state (**3t**) at the MRCISD+Q/cc-pVTZ-DK level of theory.

Geometric Trends. Important equilibrium geometric properties of the low-lying isomers are shown in Figure 2 at the composite CcCR equilibrium geometries. Mg−C equilibrium bond distances range from 2.0673 Å in the **1t** isomer to 2.2474 Å in the **4t** isomer. Qualitative similarity in bond lengths and angles for the **3s** and **3t** states is expected due to their close relative energies, especially at the CcCR level of theory. However, the carbon to diamond-vertex carbon bond lengths (C_1 or C_2 to C_3) are quite long in the diamond isomers, 1.3551 Å for the singlet state and 1.3500 Å for the triplet state. In the **3s** state, both the HOMO and LUMO (which has appreciable electron occupation in the MRCISD +Q computations) have antibonding σ and π character between the two middle carbons and the vertex carbon. In the **3t** state, the first singly occupied MO resembles the HOMO of the **3s** state, while the higher energy SOMO of the triplet has mostly Mg 3s character. The shift in electron density from the C_3 fragment to the Mg center tracks with shortening of the carbon to diamond-vertex bond lengths in the triplet state. The MOs also suggest Mg−C interactions in the **3t** state are more ionic and the Mg−C interactions in the **3s** state are more covalent, which rationalizes the multireference character of the singlet diamond isomer.

Rovibrational Properties of the $^1A_1$ Diamond Isomer (3s). The CcCR and CcCR-F12 harmonic frequencies and spectroscopic properties of the $^1A_1$ diamond isomer (**3s**) (see Figure 3) are listed in Table 5. QFF-computed results at various levels of theory for **3s** and subsequent isomers are given in the Supporting Information (Tables S4−S10). The CcCR equilibrium bond lengths $r_e(Mg-C_1)$ and $r_e(C_1-C_2)$ of the triangle base, $r_e(C_1-C_3)$ of vertex carbons, and base $\angle(C_1-Mg-C_3)$ are predicted to be 2.1533 Å, 1.3551 Å, 1.6000 Å, and 36.17°, respectively. Comparable metrics previously computed by Redondo et al. were 2.2410 Å and 2.1910 Å for the Mg−C_1 bond distance and 1.3540 and 1.3740 Å for $r_e(C_1-C_3)$ with small basis set B3LYP and MP2 computations, respectively.[31] The equilibrium geometry parameters predicted by CcCR or CcCR-F12 are clearly preferred over MP2 and B3LYP calculations.

Unfortunately, the multireference nature of the **3s** isomer causes numerical instabilities in the QFF computations. Problems were encountered in the calculation of the QFF and, in fact, the potential energy surface of the **3s** isomer. While it was possible to obtain a sensible quadratic force field, the behavior of the potential along a normal mode corresponding to ω_3, the symmetric Mg−C_1/C_3−C_2 bending mode, is pathological. The electronic structure at the calculated equilibrium structure is not unreasonable. To repeat from the earlier section, the largest t_2 excitation amplitude is 0.303, corresponding to the HOMO → LUMO excitation, with both orbitals having a_1 symmetry. This excitation amplitude is changing very rapidly in the equilibrium region and grows to nearly double this magnitude within q = 1, where q is the dimensionless normal coordinate associated with ω_3. This is a small displacement (the curve leads to a gain in the zero-point energy of the mode in the harmonic approximation), which is very much in the "Franck-Condon region". As a result, the (T) correction to the energy rapidly becomes problematic, and the potential plunges not far beyond this point (Figure 4). The rapid decay of the amplitude with increasing q reveals a rapid onset of the biradical character not far away from the minimum

https://doi.org/10.1021/acs.jpca.2c01340
J. Phys. Chem. A 2022, 126, 4132−4146

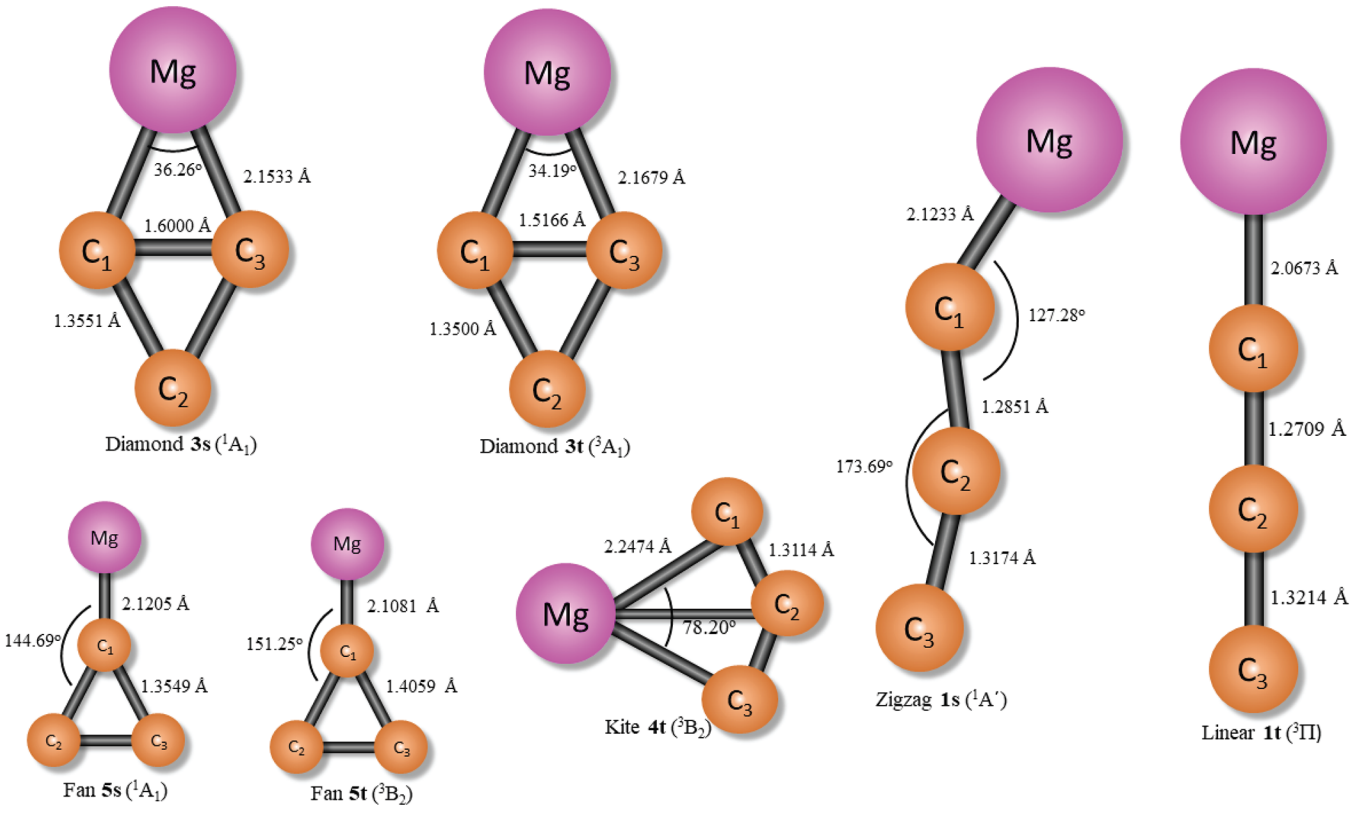

Figure 2. Equilibrium geometries for the lowest-energy isomers of MgC_3 (**3s, 3t, 1s, 5s**) at the CcCR composite geometries. Where full CcCR composite geometries had issues, the displayed geometric parameters of **1t**, **5t**, and **4t** were calculated with eq 1.

(shown at $q = 0$) and causes the perturbative triples correction in CCSD(T) to fail catastrophically. While issues qualitatively similar to this are known to occur when CCSD(T) theory is used to "break bonds", the onset of such behavior in the neighborhood of an equilibrium geometry of a closed-shell molecule is certainly unusual. In any event, it confounds all attempts to compute the vibrational frequencies of this system with VPT2 and, in fact, calls into question the quality of the harmonic frequency of ω_3. A more quantitative treatment of the vibrational levels of this molecule demands an explicitly multireference treatment, although equation-of-motion CC theory (in the double-ionization or double-electron-attachment) variants offer another valid approach to the problem at hand. When computing QFF spectroscopic constants at all levels of theory except CCSD(T)/aug-cc-pVDZ, the multireference character manifests as an unphysical positive anharmonic correction for the ν_3 symmetric C−C−Mg bending mode. Harmonic force fields (HFFs) were able to be computed for all levels of theory, but the CCSD(T)/aug-cc-pV5Z HFF also has a strange ω_3 value, which throws off the composite CcCR ω_3 value. Similar behavior has been observed in other molecules with cyclopropyl moieties.[62,92]

As previously mentioned, when single root MRCISD+Q computations were run, the **3s** isomer shows strong mixing between the HF reference configuration and the configuration corresponding to the HOMO → LUMO excitation. Surprisingly, when a two-root MRCISD+Q computation is performed, the ground state acquires mostly biradical, open-shell singlet behavior (magnitude of CI coefficient = 0.59), while the HF reference wave function had a CI coefficient magnitude of only 0.13! Figure 5 depicts the energy scan along q (again, the dimensionless normal coordinate associated with ω_3) but with the first two A_1 roots at the MRCISD+Q/cc-pVTZ-DK level of theory. At the ground state equilibrium geometry, the vertical excitation energy to the first excited A_1 state is 45.9 kcal mol^{-1}. The adiabatic excitation energy between the two states is 28.1 kcal mol^{-1}, though note that in Figure 5, the lowest-energy point for the excited A_1 state is not the equilibrium geometry of that state. The equilibrium geometry of the first A_1 excited state of the **3s** isomer is shown in Figure 6. The vertex carbon bond length, $r_e(C_1-C_3)$, only contracts from 1.6198 to1.4556 Å, while the Mg−C bond length contracts from 2.2022 to 1.9765 Å. At the 2 A_1 state MRCISD+Q optimized geometry, the vertical de-excitation energy is computed to be only 8.4 kcal mol^{-1}, which is extraordinary considering the small geometric perturbation. Even more unusual, the leading CI coefficient of the excited state corresponds to the HF configuration, with a magnitude of 0.85. Hopefully, the reader is convinced that the electronic structure of the **3s** isomer is unexpectedly onerous. Still, MRCISD+Q/cc-pVTZ-DK harmonic vibrational frequencies of the **3s** isomer were computed via displacement of Cartesian coordinates in MOLPRO and provide reasonable values. There is qualitative agreement between MRCISD+Q and the CcCR QFF for all harmonic frequencies except ω_3. Anharmonic MRCISD+Q values of the **3s** isomer are approximated by applying the CCSD(T)/aug-cc-pVDZ anharmonic corrections (which was the only level of theory where reasonably well-behaved QFF spectroscopic constants were obtained) to the MRCISD+Q harmonic frequency values and provided in Table 4. While infrared spectroscopic characterization of **3s** in this manner compromises the expected level of accuracy afforded by a proper CcCR or MRCISD+Q QFF treatment, the ad hoc MRCISD+Q fundamental frequencies should be reliable.

https://doi.org/10.1021/acs.jpca.2c01340
J. Phys. Chem. A 2022, 126, 4132−4146

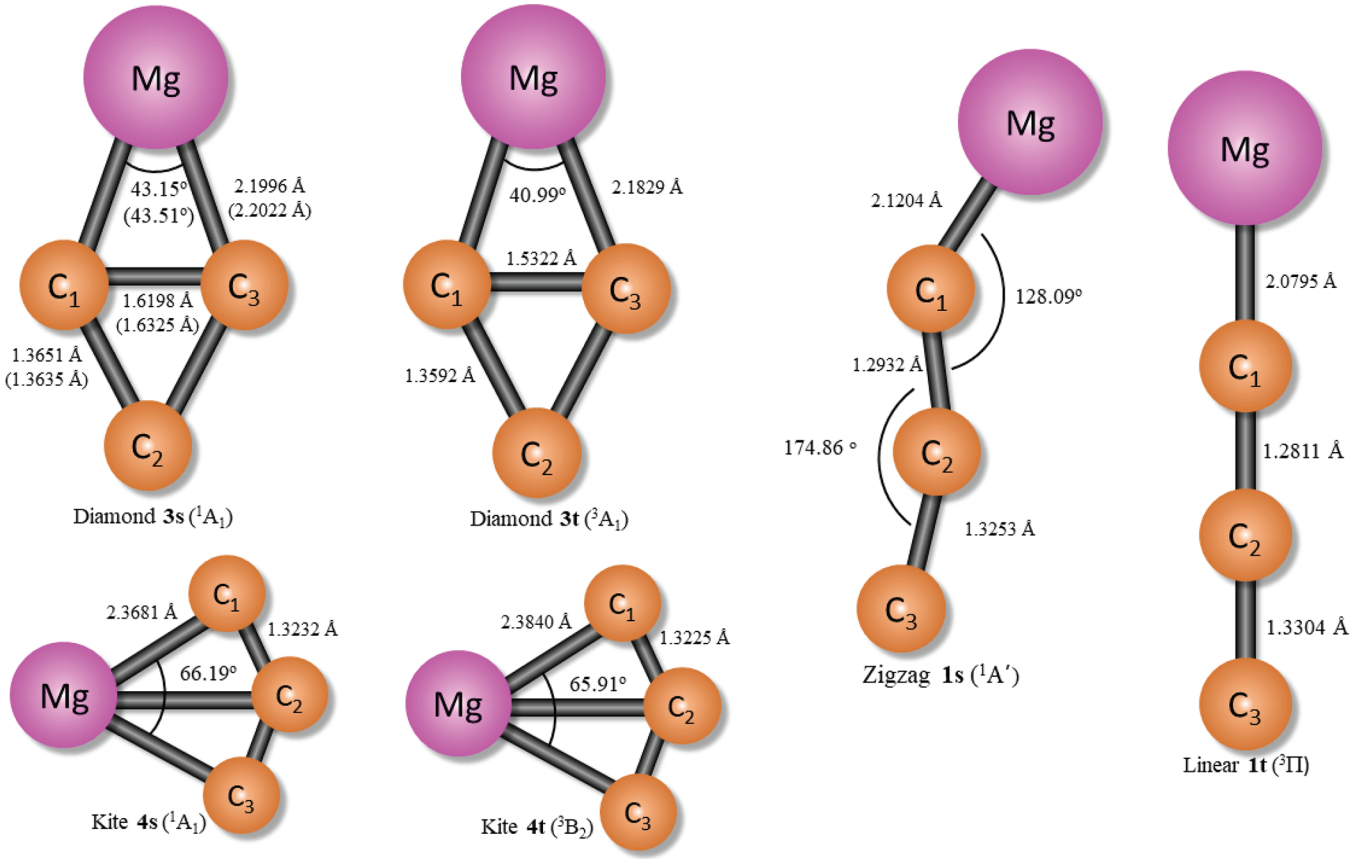

Figure 3. Optimized geometries of singlet/triplet diamond, singlet/triplet kite, and singlet zigzag of MgC_3 at the MRCISD+Q/cc-pVTZ-DK level of theory. For the **3s** isomer, the geometric parameters listed in parentheses are for the 2-state-averaged CASSCF reference MRCISD+Q computations.

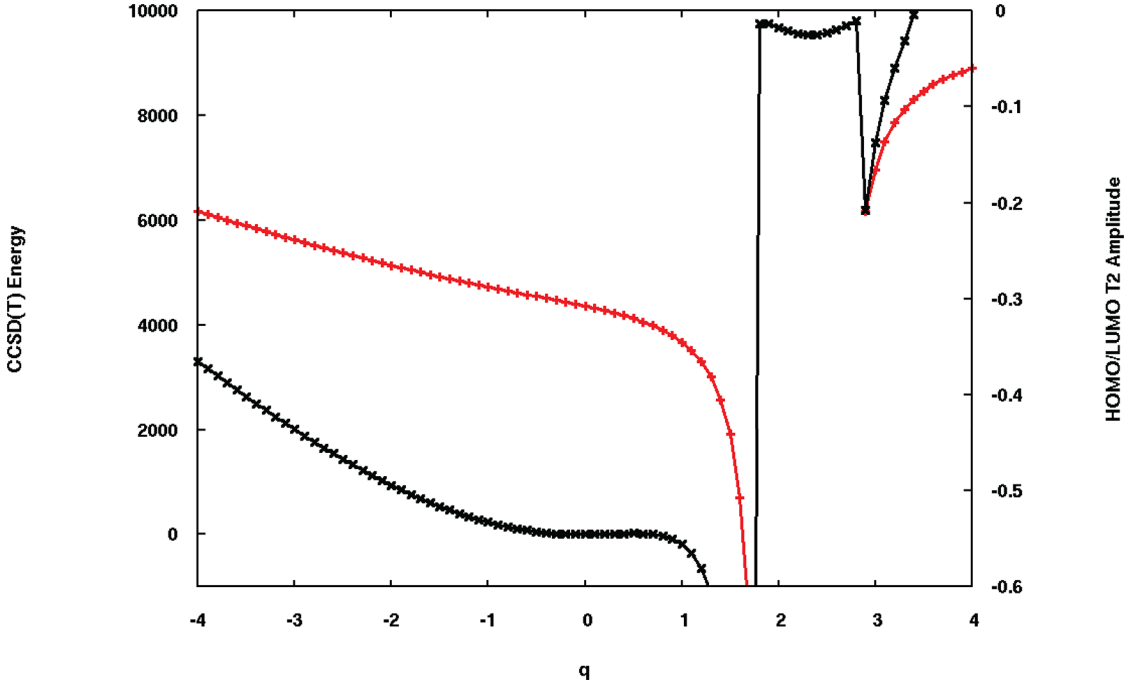

Figure 4. Variation of the CCSD(T) energy in cm^{-1} (black) along the dimensionless normal coordinate corresponding to the symmetric bending mode. The phase of the coordinate is such that the angle closes and the Mg−C distance contracts with increasing q. The largest t_2 excitation amplitude (corresponding to the diagonal HOMO → LUMO excitation) is shown in red.

https://doi.org/10.1021/acs.jpca.2c01340
J. Phys. Chem. A 2022, 126, 4132−4146

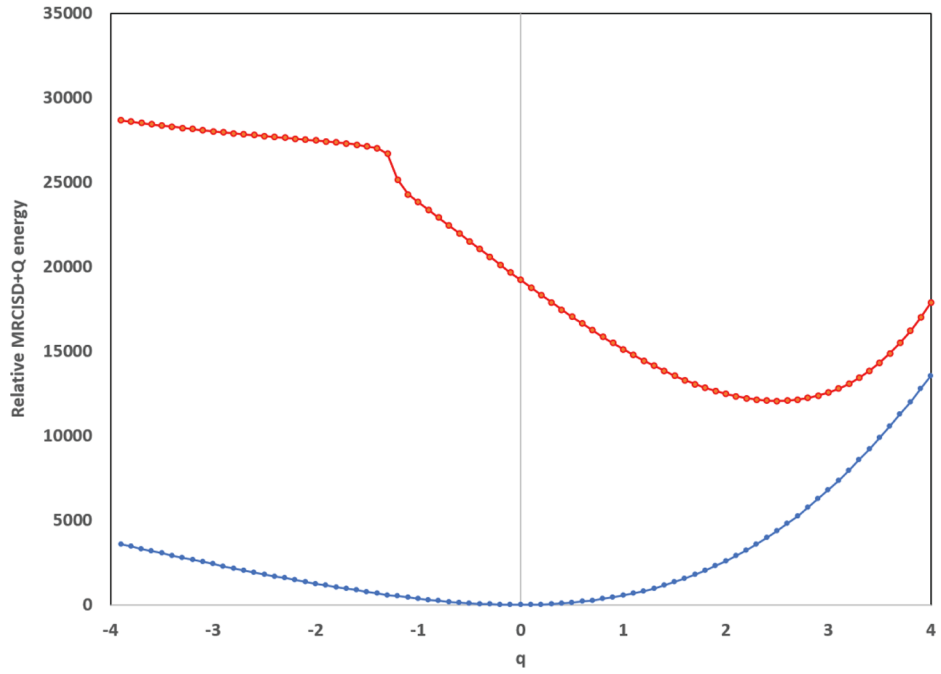

Figure 5. Variation of the MRCISD+Q energy in cm^{-1} for the two lowest A_1 states of the **3s** isomer (first root in blue, second root in red) along the dimensionless normal coordinate corresponding to the symmetric bending mode. The phase of the coordinate is such that the angle closes and the Mg−C distance contracts with increasing q.

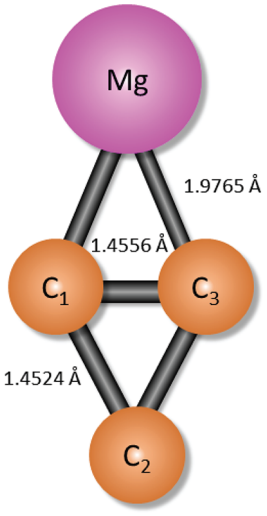

Figure 6. Optimized geometry of the first excited state of the **3s** isomer of MgC_3 at the MRCISD+Q/cc-pVTZ-DK level of theory using a 2-state-averaged CASSCF wave function.

Additionally, higher-order spectroscopic properties can be reasonably derived from the quadratic and cubic force CcCR/CcCR-F12 constants. In Table 5, CcCR and CcCR-F12 spectroscopic properties are reported from VPT2 analysis of the cubic force field (CFF) for the singlet diamond isomer.

The 4.5 D dipole moment for the **3s** isomer, computed at the MP2/aug-cc-pVDZ level of theory, is seemingly large, which implies this isomer may be detected via radio observation. However, proper accounting for multireference character in the **3s** isomer dampens the computed value of the permanent dipole moment; it still has a significant magnitude but is only 2.4 D at the MRCISD+Q/cc-pVTZ-DK level of theory. The CcCR and CcCR-F12 vibrationally averaged bond lengths of $r_0(Mg-C_1)$ are predicted to be 2.0813 and 2.0885 Å, $r_0(C_1-C_1)$ is predicted to be 1.3376 and 1.3377 Å, and the C_1-Mg-C_3 bond angles are 40.26 and 39.63°, respectively, as shown in Table 5. Computed B_0 and C_0 values (5636 and 4694 MHz, respectively, from the CcCR CFF) for this near-prolate isomer should be useful for experimental identification. The ω_3 (Mg−C−C symmetric bend) frequency at 580.1 cm^{-1} is predicted to have the highest IR intensity (74.0 $km \cdot mol^{-1}$) from the MRCI calculations. At the MP2/aug-cc-pVDZ level of theory, both the magnitude of ω_3 (706.7 cm^{-1}) and its intensity (548.0 kcal mol^{-1}) are substantially larger. The MRCISD+Q results are assumed to be more reliable for this multireference electronic state. Furthermore, this significant difference in IR intensities between MRCI and MP2 results is not observed in the triplet diamond **3t** isomer. Overall, the spectroscopic results should be more accurate than those reported previously. Additional spectroscopic constants from individual levels of theory that contribute to the CcCR/CcCR-F12 composite force field results (quartic, cubic, or harmonic depending on what was available) are provided in the Supporting Information (SI).

Rovibrational Properties of the $^3A_1$ Diamond Isomer (3t). Equilibrium bond distances of the **3t** isomer at the CcCR level of theory are 2.1678 Å for $r_e(Mg-C_1)$, 1.3498 Å for the two $C-C_{vertex}$ bonds, and 34.19° for the C_1-Mg-C_3 bond angle. Computations performed by Redondo et al. gave 2.2030 and 2.1970 Å for the $Mg-C_1$ bond distance and 1.3660 and 1.3570 Å for the $C-C_{vertex}$ bond distance at MP2 and B3LYP levels of theory, respectively.[30,31] Table 4 shows harmonic and anharmonic vibrational frequencies for the $^3A_1$ diamond **3t** at CcCR and CcCR-F12 levels of theory. Harmonic frequencies compare reasonably well with previous values reported by Redondo et al.

As the **3t** isomer does not show salient multireference character, rovibrational properties from the CcCR and CcCR-F12 QFFs are listed in Table 5 and provide necessary data to guide experimental characterization. A kinetic profile of

https://doi.org/10.1021/acs.jpca.2c01340
J. Phys. Chem. A 2022, 126, 4132−4146

Table 4. Harmonic and Anharmonic (QFF) Vibrational Frequencies and Zero-Point Energies of the Lowest-Energy Isomers

	diamond ($^1A_1$) **3s**			diamond ($^3A_1$) **3t**			linear ($^3\Pi$)[c] **1t**		zigzag ($^1A'$) **1s**		
	MRCI[a]	CcCR	CcCR-F12	MRCI	CcCR	CcCR-F12	CcCR	CcCR-F12	MRCI	CcCR	CcCR-F12
ω_1 (cm^{-1})	1519.6	1513.1	1519.3	1561.3	1607.3	1602.7	1847.6	1850.9	1838.6	1816.4	1815.8
ω_2 (cm^{-1})	1192.4	1222.0	1240.8	1161.0	1229.8	1229.5	1227.5	1228.7	1180.2	1196.6	1196.8
ω_3 (cm^{-1})	580.1	171.7	316.4	848.9	875.7	875.8	424.0	424.8	471.0	473.7	473.5
ω_4 (cm^{-1})	415.6	436.6	430.2	439.2	445.4	445.1	402.9/285.7	400.5/286.3	347.2	340.4	340.5
ω_5 (cm^{-1})	308.6	316.4	314.3	284.4	287.5	286.7	107.0/99.0	105.9/101.2	210.1	199.0	198.7
ω_6 (cm^{-1})	279.7	282.1	283.1	234.0	234.9	234.4			88.2	94.1	92.7
ν_1 (cm^{-1})	1490.4			1525.4	1571.4	1571.3			1798.7	1777.2	1777.9
ν_2 (cm^{-1})	1158.0			1124.7	1193.3	1193.2			1172.4	1188.7	1188.8
ν_3 (cm^{-1})	524.0			819.6	846.5	845.7			455.9	461.0	461.8
ν_4 (cm^{-1})	366.1			422.2	427.0	425.9			335.9	330.1	328.1
ν_5 (cm^{-1})	302.3			273.5	275.7	274.5			205.7	199.0	209.3
ν_6 (cm^{-1})	260.1			233.4	237.5	228.4			82.4	88.8	86.9
zero-point[b]	2148.0			2264.4	2322.8	2319.4			2067.7	2045.8	2047.1

[a]MRCI anharmonic frequencies are obtained based on aug-cc-pVDZ CCSD(T) anharmonic corrections. [b]Zero-point energy of harmonic frequencies. [c]For the Π electronic states, which exhibit Renner−Teller splitting in the quadratic bending force constants, each A′ component is followed by its A″ counterpart separated by a slash.

Table 5. Spectroscopic Constants Obtained from QFF Computations for the Diamond ($^3A_1$) 3t and Zigzag ($^1A'$) 1s and at CFF for Diamond ($^1A_1$) 3s Isomers

	diamond ($^1A_1$) **3s**		diamond ($^3A_1$) **3t**		zigzag ($^1A'$) **1s**	
	CcCR	CcCR-F12	CcCR	CcCR-F12	CcCR	CcCR-F2
$r_e(Mg-C_1)$ (Å)	2.1533	2.1558	2.1678	2.1690	2.1233	2.1230
$r_e(C_1-C_2)$ (Å)	1.3551	1.3551	1.3498	1.3500	1.2851	1.2847
$r_e(C_1-C_3)$ (Å)	1.6000	1.6033	1.5166	1.5167	1.3174	1.3179
$\theta_e(C_1-Mg-C_3)$ (deg)	36.26	36.22	34.19	34.18		
$\tau_e(Mg-C_1-C_2-C_3)$ (deg)	180.00	180.00	0.00	0.00	0.00	0.00
$\theta_e(C_1-C_2-C_3)$ (deg)	53.82	53.72	55.74	55.73	173.67	173.77
$\theta_e(C_2-C_1-Mg)$ (deg)					127.28	127.7
A_e (MHz)	32902.2	32841.8	36611.4	36603.4	58397.9	59306.0
B_e (MHz)	5615.3	5606.5	5432.5	5427.2	2953.0	2943.3
C_e (MHz)	4796.6	4789.0	4730.6	4726.4	2810.8	2804.1
D_{JK} (MHz)	0.002	0.002	0.041	0.041	−0.889	−0.935
D_J (MHz)	0.022	0.021	0.002	0.002	0.004	0.004
D_K (MHz)	0.336	0.291	0.200	0.200	57.446	62.463
d_1 (MHz)	-4.440×10^{-4}	-4.520×10^{-4}	-3.656×10^{-4}	-3.646×10^{-4}	-7.530×10^{-4}	-7.580×10^{-4}
d_2 (MHz)	-7.800×10^{-5}	-8.000×10^{-5}	-7.840×10^{-5}	-7.850×10^{-5}	-9.000×10^{-6}	-9.000×10^{-6}
Δ_{JK} (MHz)	0.003	0.003	0.040	0.040	−0.889	−0.935
Δ_J (MHz)	0.021	0.020	0.003	0.003	0.004	0.005
Δ_K (MHz)	0.336	0.291	0.201	0.201	57.446	62.463
δ_J (MHz)	4.440×10^{-4}	4.520×10^{-4}	3.656×10^{-4}	3.646×10^{-4}	7.530×10^{-4}	7.580×10^{-4}
δ_K (MHz)	0.021	0.022	0.028	0.028	0.028	0.028
H_{JK} (Hz)	0.001	0.002	−0.329	−0.334	5.473	6.535
H_J (Hz)	−0.319	−0.285	7.430×10^{-5}	7.360×10^{-5}	0.029	0.029
H_{KJ} (Hz)	−82.342	−56.536	−1.204	−1.221	−2915.178	−3337.586
H_K (Hz)	−2.175	−1.540	1.583	1.597	205321.826	241229.131
h_1 (Hz)	1.153×10^{-3}	1.082×10^{-3}	6.720×10^{-5}	6.450×10^{-5}	9.343×10^{-3}	9.257×10^{-3}
h_2 (Hz)	3.800×10^{-5}	3.800×10^{-5}	-2.083×10^{-4}	-2.142×10^{-5}	3.590×10^{-4}	3.560×10^{-4}
h_3 (Hz)	1.170×10^{-4}	1.080×10^{-4}	8.900×10^{-5}	8.910×10^{-5}	1.130×10^{-4}	1.150×10^{-4}
A_0 (MHz)	27702.3	28150.5	36406.9	36397.7	61978.7	63286.7
B_0 (MHz)	5635.8	5631.6	5395.4	5390.0	2935.0	2923.1
C_0 (MHz)	4693.9	4700.6	4693.0	4688.8	2794.4	2786.1
$r_0(Mg-C_1)$ (Å)	2.0813	2.0885	2.1811	2.1822	2.1320	2.1318
$r_0(C_1-C_2)$ (Å)	1.3376	1.3377	1.3569	1.3571	1.2894	1.2890
$r_0(C_1-C_3)$ (Å)	1.5387	1.5478	1.5233	1.5234	1.3246	1.3251
$\theta_0(C_2-Mg-C_3)$ (deg)	40.26	39.63	34.40	34.40		
$\theta_0(C_1-C_2-C_3)$ (deg)	53.82	53.78	55.83	55.83	167.90	167.89
$\theta_0(C_2-C_1-Mg)$ (deg)					128.16	128.72

https://doi.org/10.1021/acs.jpca.2c01340
J. Phys. Chem. A 2022, 126, 4132−4146

Table 6. Harmonic Frequencies (in cm^{-1}) and Their Intensities (in kcal mol^{-1}) Dipole Moment for Three Lowest-Energy Isomers of MgC_3

mode	symmetry	MRCI frequency	MRCI intensity	MP2 frequency	MP2 intensity
diamond ($^1A_1$) **3s**					
ω_1	A_1	1519.6	10.8	1526.2	49.4
ω_2	B_1	1192.4	2.3	1311.4	1.6
ω_3	A_1	580.1	74.0	706.7	548.0
ω_4	A_1	415.6	53.8	414.5	13.0
ω_5	B_1	308.6	43.1	372.8	53.1
ω_6	B_2	279.7	0.0	324.4	18.0
μ		2.4 D		4.5 D	
diamond ($^3A_1$) **3t**					
ω_1	A_1	1561.3	4.6	1581.9	21.8
ω_2	B_1	1161.0	0.4	1258.1	1.3
ω_3	A_1	848.9	8.5	830.2	0.7
ω_4	A_1	439.2	113.7	423.4	101.3
ω_5	B_1	284.4	28.0	269.1	24.2
ω_6	B_2	234.0	0.0	226.9	0.1
μ		2.0 D		2.4 D	
zigzag ($^1A'$) **1s**					
ω_1	A'	1838.6	254.7	1885.8	288.6
ω_2	A'	1180.2	65.0	1179.6	18.6
ω_3	A'	471.0	65.6	473.5	27.0
ω_4	A'	347.2	9.9	337.1	1.9
ω_5	A''	210.1	0.0	178.6	9.8
ω_6	A'	88.2	4.0	127.7	8.6
μ		5.8 D		6.3 D	
linear ($^3\Pi$) **1t**					
ω_1	σ			2392.7	571.1
ω_2	σ			1215.2	288.3
ω_3	σ			428.2	121.9
ω_4	π			2077.7/481.2	18.7/12.3
ω_5	π			144.2/101.2	2.3/0.4
μ		6.1 D		6.4 D	

transition states converting between isomers of MgC_3 is outside the scope of this work. Until such data are available, it can be assumed that population of the **3t** isomer may be accessible in cold, dark astrochemical environments such as molecular clouds. Similar to the equilibrium geometries, the CcCR values of 2.1811 Å computed for $r_0(Mg-C_1)$ and 1.3569 Å computed for $r_0(C_1-C_2)$ are different enough from the **3s** isomer for pure rotational experiments to resolve both spin multiplicities if they exist in equilibrium. Table 6 shows the permanent dipole moment of the triplet diamond isomer is 2.4 D with MP2 and 2.0 with MRCISD+Q. Both values are less than that of the **3t** isomer but still reasonably large. The **3t** isomer is also near-prolate, with CcCR values of B_0 and C_0 computed to be 5395.3 and 4693.0 MHz, respectively. Interestingly, the **3t** CcCR/CcCR-F12 C_0 values are within 15.0 MHz of the respective **3s** C_0 values. The B_0 values for the **3t** isomer are fortunately ~300 MHz lower.

Compared to the discrepancies between MRCISD+Q and MP2 observed in the computation of **3s** IR intensities, both levels of theory qualitatively show the magnesium−carbon stretch ω_4 has the largest IR intensity of **3t**, with the MRCISD +Q frequency at 439.2 cm^{-1} showing an intensity of 113.7 km·mol^{-1}. Again, this rather good agreement can be attributed to the more single-reference nature of the **3t** isomer. From the composite QFF, the VPT2 input necessitates inclusion of 3-fold Fermi resonance polyads for $\nu_2 = 2\nu_3 = \nu_3 + \nu_4$ and $\nu_3 = 2\nu_5 = 2\nu_6$ in addition to a type-2 Fermi resonance for $\nu_1 = \nu_2 + \nu_4$ as well as a ν_5/ν_6 Coriolis resonance. Fermi and Coriolis resonances are incorporated in the VPT2 calculations to increase the accuracy of the anharmonic results.[93,94] Generally, whether the Fermi resonances are treated individually or coupled via polyads, the magnitudes of fundamental vibrational frequencies differ by only −5.2 to +11.0 cm^{-1}. Table S2 displays minor differences in the resonance treatment, while polyad-corrected fundamental frequencies are reported in Table 4 for both the **3t** and **1s** isomers. At this point, the MRCISD+Q/cc-pVTZ-DK harmonic zero-point vibrational energies (ZPVEs) can be used to correct relative energies between the $^1A_1$ diamond and $^3A_1$ diamond isomers. A relative energy shift of 0.33 kcal mol^{-1} occurs, further favoring the **3s** isomer as the true lowest-energy isomer.

Finally, we have neglected to computationally explore the fine structure of any of the triplet isomers of MgC_3. The open-shell character of the triplet isomers will show clearly noticeable differences in their rotational/rovibrational spectroscopy. Spin−spin and spin−rotation interactions may be important features to distinguish between singlet and triplet isomers both in terrestrial experiments and astrochemical observation but are outside the scope of this work.

Rovibrational Properties of the ($^1A'$) Zigzag Isomer (1s). For the ($^1A'$) zigzag isomer (**1s**), equilibrium geometry parameters are computed to be 1.2851 Å for the C_1-C_2 bond distance as shown in Figure 1, while the $r_e(Mg-C_1)$ bond distance is 2.1233 Å at the CcCR level of theory. The previous

https://doi.org/10.1021/acs.jpca.2c01340
J. Phys. Chem. A 2022, 126, 4132−4146

work by Redondo et al. generally shows good agreement with the present higher-level results.[31] In Table 4, the harmonic vibrational frequencies are given for MRCISD+Q, CcCR, and CcCR-F12 approaches, while the QFF fundamental frequencies are given for CcCR and CcCR-F12. The MRCI ω_1 value shows the largest difference (~22.5 cm^{-1}) compared to CcCR and CcCR-F12. The rest of the vibrational frequencies, however, are in good agreement, with the exception of ν_5, which exhibits a 6.7 cm^{-1} difference between MRCI and CcCR. There are positive anharmonicities in ν_3 and ν_4 shifting the values to 461.0 and 330.1 cm^{-1}, respectively, for the CcCR QFF, which is a common behavior in pseudolinear species.[66,95] With a dipole moment of 6.3/5.8 D, computed at the MP2/aug-cc-pVDZ and MRCISD+Q/cc-pVTZ-DK levels of theory, respectively, the **1s** isomer also has good prospects for being rotationally detected in the ISM. The CcCR QFF spectroscopic constants will guide future gas phase experiments and astronomical analysis for observation of MgC_3 in this isomeric form.

Rovibrational Properties of the Linear ($^3\Pi$) Isomer (1t). Composite geometric parameters of the triplet linear ($^3\Pi$) state are shown in Figure 2. The CcCR equilibrium bond distances are predicted to be 2.0673 Å for Mg−C_1 and 1.2709 Å for C_1−C_2. These geometric parameters show good agreement with the previous work by Redondo et al.[31] The linear ($^3\Pi$) isomer (**1t**) appears to be the second lowest-energy isomer (Table 2). Computed dipole moments for the triplet linear isomer (**1t**) are the largest of the low-lying isomers, meaning it could be detected via radio telescopes provided that sufficient spectral data are on hand for comparison.

Unfortunately, VPT2 is not reliable for Renner−Teller systems, and only harmonic vibrational frequencies for the **1t** isomer are reported with CCSD(T) and CCSD(T)-F12b levels of theory. MRCISD+Q harmonic bending frequencies (from both Cartesian and internal coordinate displacements) were spuriously large possibly due to vibronic coupling with a low-lying Σ state. Therefore, harmonic frequencies are reported in Table 4 only using the CcCR and CcCR-F12 composite approaches.

Renner−Teller splitting was observed with the MP2/aug-cc-pVDZ computations computed in Gaussian16 with analytic second derivatives and reported in Table 6. However, yet another numerical artifact arose as the Renner−Teller effect does not seem compatible with the low level of theory employed, and the ω_4 mode was anomalously split by nearly 1600 cm^{-1}. Redondo et al. also observed a huge Renner−Teller splitting of the C−C−C bending mode (ω_4) at the MP2(full)/6-311G(d) level of theory.[31] When they used B3LYP/6-311G(d), a large Renner−Teller splitting for ω_4 (175 cm^{-1}) was observed, though this is certainly attenuated compared to MP2 results. The CcCR/CcCR-F12 harmonic frequencies computed here do not show large spurious Renner−Teller splitting values. A Renner−Teller splitting of ~115−140 cm^{-1} is observed for C−C−C out-of-plane bending. The degeneracy of the Mg−C−C bending modes (ω_5) is also lifted due to orbital angular momentum in the $^3\Pi$ state, with a Renner−Teller splitting of only 4.7−8.0 cm^{-1} observed.

If the $^3\Pi$ isomer was confirmed to be the ground state of MgC_3, it would be worth pursuing a treatment of non-Born−Oppenheimer effects, as described by Jutier,[96] Perić,[97,98] and others.[99] Given that VPT2 is problematic when any Born−Oppenheimer breakdown exists in the vibrational wave function and that spin−orbit coupling effects have also been ignored, the given harmonic force fields for the **1t** isomer should still be valuable reference data. It is clear that many isomers of MgC_3 pose a severe challenge for conventional *ab initio* techniques, and hopefully this work inspires experimental spectroscopic investigation.

Bond Dissociation Energy. The bond dissociation energies (BDEs) of the C_3 fragment from the Mg metal are computed at CcC and CcCR levels of theory and given in Table 7. Note that the BDE of singlet isomers is relative to Mg + $^1C_3$, while the BDE of triplet isomers is relative to Mg + $^3C_3$. The CcCR BDEs are predicted to be 78.3 kcal mol^{-1}, 26.9 kcal mol^{-1}, 75.5 kcal mol^{-1}, and 23.3 kcal mol^{-1} for **3t**, **3s**, **1t**, and **1s**, respectively. While the singlet isomers are computed to be lower in energy, photoexcitation of either Mg atoms or C_3 could allow triplet isomers of MgC_3 to associate and then relax into their more thermodynamically stable forms. The triplet BDEs are comparable to typical covalent bonds including the Mg−C bond strengths of ~80 kcal mol^{-1} for the astrochemically known magnesium acetylides. The computed BDE strengths of both spin multiplicities imply that these isomers are stable, can be synthesized in the lab, and may likely be observable in circumstellar media. Thermal processes would have to range above 14000 K for even the **3t** isomer to dissociate its Mg atom implying that these molecules could certainly be present in the halo of carbon-rich stars like IRC +10216. Additionally, these molecules could serve as observational temperature gauges if they, first, are present in such environments and, second, have a clear distance approaching the star where they are no longer observed.

Table 7. Bond Dissociation Energy (kcal mol^{-1}) of MgC_3 at CcC and CcCR Levels of Theory

		CcC	CcCR
diamond ($^3A_1$)	**3t**	78.6	78.3
diamond ($^1A_1$)	**3s**	27.6	26.9
linear ($^3\Pi$)	**1t**	75.7	75.5
zigzag ($^1A'$)	**1s**	23.6	23.3

CONCLUSIONS

All relevant low-energy isomers of magnesium tricarbide have been investigated with rigorous levels of theory and several basis sets to the furthest extent possible. The CcCR relative energies are as follows (in kcal mol^{-1}): 0.0 (**3t**) < 0.3 (**3s**) < 2.8 (**1t**) < 4.3 (**1s**) < 7.1 (**4s**) < 9.6 (**6t**) < 17.1 (**6s**). Additionally, the MgC_3 molecule poses a formidable challenge for theoretical rovibrational spectroscopy. Post-CCSD(T) corrections to CcCR and MRCISD+Q calculations verify the true ordering of the low-lying MgC_3 isomers to be **3s** < **3t** < **1t** < **1s**.

Our coupled cluster-based composite approaches have previously been adapted for computing QFFs of transition metal-containing molecules. Yet, QFFs require additional modifications to handle this tricky s-block metal-containing species. Even then, the computation of anharmonic rovibrational spectroscopic constants has not been entirely successful. Highly accurate QFF-derived constants were obtained for the triplet diamond (**3t**) and singlet zigzag (**1s**) isomers. However, due to numerical instabilities in the QFF, only a cubic force field (CFF) was provided for the ground state singlet diamond

https://doi.org/10.1021/acs.jpca.2c01340
J. Phys. Chem. A 2022, 126, 4132−4146

isomer (**3s**), and harmonic vibrational frequencies were computed via CcCR and CcCR-F12 for the $^3\Pi$ isomer (**1t**).

While rovibrational properties computed with CcCR-F12 and CcCR are known to give fundamental vibrational frequencies to within 5 cm^{-1} of experimental results for organic species,[100] the accuracy of computed properties for MgC_3 will need to be verified by experimental groups. However, our spectroscopic constants are significantly more reliable than those determined in previous studies. If multiple isomers exist in equilibrium, the symmetric C−Mg−C bend of the **3s** ground state (ν_3) should be easily identified since it has a significantly different fundamental frequency compared to any vibrational mode from other low-lying isomers. Four low-lying isomers (**1t** > **1s** > **3s** > **3s**) have dipole moments greater than 2.0 D, suggesting they will be rotationally visible if present in the ISM or in circumstellar envelopes. The challenging electronic structure of MgC_3 has been revealed in enough detail to guide terrestrial characterization and astrochemical detection despite some methodological bottlenecks.

■ ASSOCIATED CONTENT

Supporting Information

The Supporting Information is available free of charge at https://pubs.acs.org/doi/10.1021/acs.jpca.2c01340.

Symmetrized internal coordinates of various isomers, MO diagrams for isomers, and data used in computing CcCR and CcCR-F12 (PDF)

■ AUTHOR INFORMATION

Corresponding Author

Nathan J. DeYonker − *Department of Chemistry, University of Memphis, Memphis, Tennessee 38151, United States;* orcid.org/0000-0003-0435-2006; Email: ndyonker@memphis.edu

Authors

Donatus A. Agbaglo − *Department of Chemistry, University of Memphis, Memphis, Tennessee 38151, United States*

Qianyi Cheng − *Department of Chemistry, University of Memphis, Memphis, Tennessee 38151, United States;* orcid.org/0000-0002-4640-2238

Ryan C. Fortenberry − *Department of Chemistry & Biochemistry, University of Mississippi, University, Mississippi 38677-1848, United States;* orcid.org/0000-0003-4716-8225

John F. Stanton − *Department of Chemistry and Physics, University of Florida, Gainesville, Florida 32611, United States*

Complete contact information is available at: https://pubs.acs.org/10.1021/acs.jpca.2c01340

Notes

The authors declare no competing financial interest.

■ ACKNOWLEDGMENTS

The High Performance Computing Center and the Computational Research On Materials Institute at The University of Memphis (CROMIUM) provided generous resources for this research. R.C.F. is grateful for funding from NASA grant number NNX17AH15G, NSF grant OIA-1757220, and startup funding provided by the University of Mississippi. J.F.S. has been financially supported by the U.S. Department of Energy, Office of Basic Energy Sciences under Award DE-SC0018164. We thank Dr. Timothy J. Lee (NASA Ames) and Prof. Kirk A. Peterson (Washington State) for advice providing technical advice.

■ REFERENCES

(1) Kloska, K. A.; Fortenberry, R. C. Gas-phase spectra of MgO molecules: a possible connection from gas-phase molecules to planet formation. *Mon. Not. R. Astron. Soc.* **2018**, *474*, 2055−2063.

(2) Adibekyan, V. Z.; Santos, N.; Sousa, S.; Israelian, G.; Mena, E. D.; Hernández, J. G.; Mayor, M.; Lovis, C.; Udry, S. Overabundance of α-elements in exoplanet-hosting stars. *Astron. Astrophys.* **2012**, *543*, A89.

(3) Adibekyan, V.; Santos, N.; Figueira, P.; Dorn, C.; Sousa, S.; Delgado-Mena, E.; Israelian, G.; Hakobyan, A.; Mordasini, C. From stellar to planetary composition: Galactic chemical evolution of Mg/Si mineralogical ratio. *Astron. Astrophys.* **2015**, *581*, L2.

(4) Grant, D. *Solid-State Hydrogen Storage*; Elsevier: 2008; pp 357−380, DOI: 10.1533/9781845694944.4.357.

(5) Kawaguchi, K.; Kagi, E.; Hirano, T.; Takano, S.; Saito, S. Laboratory spectroscopy of $MgNC^-$ The first radioastronomical identification of Mg-bearing molecule. *Astrophys. J.* **1993**, *406*, L39−L42.

(6) Guélin, M.; Lucas, R.; Cernicharo, J. MgNC and the carbon-chain radicals in IRC +10216. *Astron. Astrophys.* **1993**, *280*, L19−L22.

(7) Ziurys, L. M.; Apponi, A.; Guélin, M.; Cernicharo, J. Detection of MgCN in IRC +10216: a new metal-bearing free radical. *Astrophys. J.* **1995**, *445*, L47−L50.

(8) DeYonker, N. J. What a difference a decade has not made: the murky electronic structure of iron monocyanide (FeCN) and iron monoisocyanide (FeNC). *J. Phys. Chem. A* **2015**, *119*, 215−223.

(9) Cheng, Q.; Fortenberry, R. C.; DeYonker, N. J. Towards a quantum chemical protocol for the prediction of rovibrational spectroscopic data for transition metal molecules: Exploration of CuCN, CuOH, and CuCCH. *J. Chem. Phys.* **2017**, *147*, 234303.

(10) Fortenberry, R. C.; DeYonker, N. J. Rovibrational Quantum Chemical Treatment of Inorganic and Organometallic Astrochemicals. *Acc. Chem. Res.* **2021**, *54*, 271.

(11) Gardner, M. B.; Westbrook, B. R.; Fortenberry, R. C. Spectral characterization for small clusters of silicon and oxygen: SiO_2, SiO_3, Si_2O_3, & Si_2O_4. *Planet Space Sci.* **2020**, *193*, 105076.

(12) Doerksen, E. S.; Fortenberry, R. C. Coincidence between Bond Strength, Atomic Abundance, and the Composition of Rocky. *Materials. ACS Earth Space Chem.* **2020**, *4*, 812−817.

(13) Savage, B. D.; Sembach, K. R. Interstellar abundances from absorption-line observations with the Hubble Space Telescope. *Annu. Rev. Astron. Astrophys.* **1996**, *34*, 279−329.

(14) Palmer, C. Z.; Fortenberry, R. C. Rovibrational Considerations for the Monomers and Dimers of Magnesium Hydride and Magnesium Fluoride. *J. Chem. Phys. A* **2018**, *122*, 7079−7088.

(15) Cabezas, C.; Cernicharo, J.; Alonso, J. L.; Agúndez, M.; Mata, S.; Guelin, M.; Peña, I. Laboratory and Astronomical Discovery of HydroMagnesium Isocyanide. *Astrophy. J.* **2013**, *775*, 133.

(16) Anderson, M.; Ziurys, L. M. Laboratory detection and millimeter spectrum of the MgCCH radical. *Astrophys. J.* **1995**, *439*, L25−L28.

(17) Agúndez, M.; Cernicharo, J.; Guélin, M. New molecules in IRC +10216: confirmation of C_5S and tentative identification of MgCCH, NCCP, and SiH_3CN. *Astron. Astrophys.* **2014**, *570*, A45.

(18) Cernicharo, J.; Cabezas, C.; Pardo, J.; Agúndez, M.; Bermúdez, C.; Velilla-Prieto, L.; Tercero, F.; López-Pérez, J.; Gallego, J.; Fonfría, J. P.; et al. Discovery of two new magnesium-bearing species in IRC +10216: MgC_3N and MgC_4H. *Astron. Astrophys.* **2019**, *630*, L2.

(19) Pardo, J.; Cabezas, C.; Fonfría, J.; Agúndez, M.; Tercero, B.; de Vicente, P.; Guélin, M.; Cernicharo, J. Magnesium radicals MgC_5N and MgC_6H in IRC +10216. *Astron. Astrophys.* **2021**, *652*, L13.

(20) Anderson, M.; Steimle, T.; Ziurys, L. The millimeter and submillimeter rotational spectrum of the MgCN radical (X^2Sigma^+). *Astrophy. J.* **1994**, *429*, L41−L44.
(21) Gronowski, M.; Kołos, R. Ab initio Studies of the Structure and Spectroscopy of CHNMg Stoichiometry and van der Waals Complexes and van der Waals Complexes. *J. Chem. Phys. A* **2013**, *117*, 4455−4461.
(22) Brewster, M.; Apponi, A.; Xin, J.; Ziurys, L. Millimeter-wave spectroscopy of vibrationally-excited NaCCH ($\tilde{X}^1\Sigma^+$) and MgCCH ($\tilde{X}^2\Sigma^+$): the ν_5 bending mode. *Chem. Phys. Lett.* **1999**, *310*, 411−422.
(23) Petrie, S.; Kagi, E.; Kawaguchi, K. Has MgCCCN been detected within the envelope of IRC +10216? *Mon. Not. R. Astron. Soc.* **2003**, *343*, 209−214.
(24) Forthomme, D.; Linton, C.; Tokaryk, D.; Adam, A.; Granger, A. High-resolution laser spectroscopy of the $\tilde{A}^2\,\Pi$ - $\tilde{X}^2\,\Sigma$. transition of MgC_4H. *Chem. Phys. Lett.* **2010**, *488*, 116−120.
(25) Heath, J.; Zhang, Q.; O'Brien, S.; Curl, R.; Kroto, H.; Smalley, R. The formation of long carbon chain molecules during laser vaporization of graphite. *J. Am. Chem. Soc.* **1987**, *109*, 359−363.
(26) Gausset, L.; Herzberg, G.; Lagerqvist, A.; Rosen, B. Analysis of the 4050-Å Group of the C_3 Molecule. *Astrophys. J.* **1965**, *142*, 45.
(27) Hinkle, K. W.; Keady, J. J.; Bernath, P. F. Detection of C_3 in the circumstellar shell of IRC +10216. *Science* **1988**, *241*, 1319−1322.
(28) Rohlfing, E. A. Laser-induced-fluorescence spectroscopy of jet-cooled C_3. *J. Chem. Phys.* **1989**, *91*, 4531−4542.
(29) Clegg, R.; Lambert, D. C_3 molecules in diffuse interstellar clouds. *Mon. Not. R. Astron. Soc.* **1982**, *201*, 723−733.
(30) Zheng, X.; Wang, Z.; Tang, A. On the equilibrium structure and stability of MgC_n (n= 2−4) species. *J. Mol. Struct.* **1999**, *492*, 79−84.
(31) Redondo, P.; Barrientos, C.; Largo, A. Structures and stabilities of MgC_3 isomers: a theoretical study. *Chem. Phys. Lett.* **2001**, *335*, 64−70.
(32) Babin, M. C.; DeWitt, M.; Weichman, M. L.; DeVine, J. A.; Neumark, D. M. High-resolution anion photoelectron spectroscopy of cryogenically cooled 4-atom silicon carbides. *Mol. Phys.* **2021**, *119*, e1817596.
(33) Apponi, A.; McCarthy, M.; Gottlieb, C.; Thaddeus, P. The rotational spectrum of rhomboidal SiC_3. *J. Chem. Phys.* **1999**, *111*, 3911−3918.
(34) McCarthy, M.; Apponi, A.; Thaddeus, P. Rhomboidal SiC_3. *J. Chem. Phys.* **1999**, *110*, 10645−10648.
(35) McCarthy, M.; Apponi, A.; Gottlieb, C.; Thaddeus, P. Laboratory detection of five new linear silicon carbides: SiC_3, SiC_5, SiC_6, SiC_7, and SiC_8. *Astrophys. J.* **2000**, *538*, 766.
(36) Alberts, I. L.; Grev, R. S.; Schaefer, H. F., III Geometrical structures and vibrational frequencies of the energetically low-lying isomers of SiC_3. *J. Chem. Phys.* **1990**, *93*, 5046−5052.
(37) Yang, T.; Bertels, L.; Dangi, B. B.; Li, X.; Head-Gordon, M.; Kaiser, R. I. Gas phase formation of c-SiC_3 molecules in the circumstellar envelope of carbon stars. *Proc. Natl. Acad. Sci. U.S.A* **2019**, *116*, 14471−14478.
(38) Stanton, J. F.; Gauss, J.; Christiansen, O. Equilibrium geometries of cyclic SiC_3 isomers. *J. Chem. Phys.* **2001**, *114*, 2993−2995.
(39) Hunsicker, S.; Jones, R. Structure and bonding in mixed silicon-carbon clusters and their anions. *J. Chem. Phys.* **1996**, *105*, 5048−5060.
(40) Rintelman, J. M.; Gordon, M. S. Structure and energetics of the silicon carbide clusters SiC_3 and Si_2C_2. *J. Chem. Phys.* **2001**, *115*, 1795−1803.
(41) Sattelmeyer, K. W.; Schaefer, H. F., III; Stanton, J. F. The global minimum structure of SiC_3: The controversy continues. *J. Chem. Phys.* **2002**, *116*, 9151−9153.
(42) Bejjani, M.; Rittby, C.; Graham, W. Fourier transform infrared matrix and density functional theory study of the vibrational spectrum of the linear MgC_3^-anion. *J. Chem. Phys.* **2011**, *135*, 054513.
(43) Shavitt, I.; Bartlett, R. J. *Many-body methods in chemistry and physics: MBPT and Coupled-Cluster Theory*; Cambridge University Press: 2009; DOI: 10.1017/CBO9780511596834.
(44) Adler, T. B.; Knizia, G.; Werner, H.-J. A simple and efficient CCSD(T)-F12 approximation. *J. Chem. Phys.* **2007**, *127*, 221106.
(45) Knizia, G.; Adler, T. B.; Werner, H.-J. Simplified CCSD(T)-F12 methods: Theory and benchmarks. *J. Chem. Phys.* **2009**, *130*, 054104.
(46) Becke, A. Density-Functional Thermochemistry III. The Role of Exact Exchange. *J. Chem. Phys.* **1993**, *98*, 5648.
(47) Møller, C.; Plesset, M. S. Note on an approximation treatment for many-electron systems. *Phys. Rev.* **1934**, *46*, 618.
(48) Scuseria, H.; Robb, G.; Cheeseman, M.; Scalmani, J.; Barone, G.; Petersson, V.; Nakatsuji, H. et al. *Gaussian 16*; 2016.
(49) Yang, W.; Parr, R. G.; Lee, C. Various functionals for the kinetic energy density of an atom or molecule. *Phys. Rev. A* **1986**, *34*, 4586.
(50) Lee, C.; Yang, W.; Parr, R. G. Development of the Colle-Salvetti correlation-energy formula into a functional of the electron density. *Phys. Rev. B* **1988**, *37*, 785.
(51) Agbaglo, D.; Fortenberry, R. C. The performance of explicitly correlated wavefunctions [CCSD (T)-F12b] in the computation of anharmonic vibrational frequencies. *Chem. Phys. Lett.* **2019**, *734*, 136720.
(52) Agbaglo, D.; Lee, T. J.; Thackston, R.; Fortenberry, R. C. A Small Molecule with PAH Vibrational Properties and a Detectable Rotational Spectrum: c-$(C)C_3H_2$, Cyclopropenylidenyl Carbene. *Astrophys. J.* **2019**, *871*, 236.
(53) Huang, X.; Valeev, E. F.; Lee, T. J. Comparison of one-particle basis set extrapolation to explicitly correlated methods for the calculation of accurate quartic force fields, vibrational frequencies, and spectroscopic constants: Application to H_2O, N_2H^+, NO_2^+, and C_2H_2. *J. Chem. Phys.* **2010**, *133*, 244108.
(54) Westbrook, B. R.; Fortenberry, R. C. Anharmonic frequencies of $(MO)_2$ and related hydrides for M= Mg, Al, Si, P, S, Ca, and Ti and heuristics for predicting anharmonic corrections of inorganic oxides. *J. Chem. Phys. A* **2020**, *124*, 3191−3204.
(55) Westbrook, B. R.; del Rio, W. A.; Lee, T. J.; Fortenberry, R. C. Overcoming the out-of-plane bending issue in an aromatic hydrocarbon: the anharmonic vibrational frequencies of c-$(CH)C_3H_2^+$. *Phys. Chem. Chem. Phys.* **2020**, *22*, 12951−12958.
(56) Rittby, M.; Bartlett, R. J. An open-shell spin-restricted coupled cluster method: application to ionization potentials in nitrogen. *J. Phys. Chem.* **1988**, *92*, 3033−3036.
(57) Werner, H.; Knowles, P.; Knizia, G.; Manby, F.; Schütz, M.; Celani, P.; Györffy, W.; Kats, D.; Korona, T.; Lindh, R. et al. *MOLPRO*, version 2019.2, a package of *ab initio* programs; 2020.
(58) Hill, J. G.; Peterson, K. A. Correlation consistent basis sets for explicitly correlated wavefunctions: valence and core-valence basis sets for Li, Be, Na, and Mg. *Phys. Chem. Chem. Phys.* **2010**, *12*, 10460−10468.
(59) Prascher, B. P.; Woon, D. E.; Peterson, K. A.; Dunning, T. H.; Wilson, A. K. Gaussian basis sets for use in correlated molecular calculations. VII. Valence, core-valence, and scalar relativistic basis sets for Li, Be, Na, and Mg. *Theor. Chem. Acc.* **2011**, *128*, 69−82.
(60) Knowles, P. J.; Hampel, C.; Werner, H.-J. Coupled cluster theory for high spin, open shell reference wave functions. *J. Chem. Phys.* **1993**, *99*, 5219−5227.
(61) Douglas, M.; Kroll, N. M. Quantum electrodynamical corrections to the fine structure of helium. *Ann. Phys.* **1974**, *82*, 89−155.
(62) Fortenberry, R. C.; Lee, T. J. *Annual Reports in Computational Chemistry*; Elsevier: 2019; Vol. *15*, pp 173−202, DOI: 10.1016/bs.arcc.2019.08.006.
(63) Huang, X.; Lee, T. J. Accurate *ab initio* quartic force fields for NH_2^- and CCH^- and rovibrational spectroscopic constants for their isotopologs. *J. Chem. Phys.* **2009**, *131*, 104301.
(64) Huang, X.; Lee, T. J. A procedure for computing accurate *ab initio* quartic force fields: Application to HO_2^+ and H_2O. *J. Chem. Phys.* **2008**, *129*, 044312.
(65) Kitchens, M. J.; Fortenberry, R. C. The rovibrational nature of closed-shell third-row triatomics: and HXO, X= Si^+, P, S^+, and Cl. *Chem. Phys.* **2016**, *472*, 119−127.

https://doi.org/10.1021/acs.jpca.2c01340
J. Phys. Chem. A 2022, 126, 4132−4146

(66) Fortenberry, R. C.; Huang, X.; Francisco, J. S.; Crawford, T. D.; Lee, T. J. The trans-HOCO radical: Quartic force fields, vibrational frequencies, and spectroscopic constants. *J. Chem. Phys.* **2011**, *135*, 134301.
(67) Theis, R. A.; Fortenberry, R. C. Trihydrogen cation with neon and argon: structural, energetic, and spectroscopic data from quartic force fields. *J. Phys. Chem. A* **2015**, *119*, 4915−4922.
(68) Kutzelnigg, W.; Morgan, J. D., III Rates of convergence of the partial-wave expansions of atomic correlation energies. *J. Chem. Phys.* **1992**, *96*, 4484−4508.
(69) Martin, J. M. Ab initio total atomization energies of small moleculestowards the basis set limit. *Chem. Phys. Lett.* **1996**, *259*, 669−678.
(70) Martin, J. M.; Lee, T. J. The atomization energy and proton affinity of NH_3. An *ab initio* calibration study. *Chem. Phys. Lett.* **1996**, *258*, 136−143.
(71) Kállay, M.; Surján, P. R. Higher excitations in coupled-cluster theory. *J. Chem. Phys.* **2001**, *115*, 2945−2954.
(72) Werner, H.; Knowles, P.; Knizia, G.; Manby, F.; Schütz, M. Molpro: a general-purpose quantum chemistry program package. *Wiley Interdiscip. Rev.: Comput. Mol. Sci.* **2012**, *2*, 242−253.
(73) Knowles, P. J.; Handy, N. C. A new determinant-based full configuration interaction method. *Chem. Phys. Lett.* **1984**, *111*, 315−321.
(74) Knowles, P. J.; Werner, H.-J. An efficient second-order MC SCF method for long configuration expansions. *Chem. Phys. Lett.* **1985**, *115*, 259−267.
(75) Werner, H.-J.; Knowles, P. J. A second order multiconfiguration SCF procedure with optimum convergence. *J. Chem. Phys.* **1985**, *82*, 5053−5063.
(76) Amos, R. D.; Andrews, J. S.; Handy, N. C.; Knowles, P. J. Open-shell Møller—Plesset perturbation theory. *Chem. Phys. Lett.* **1991**, *185*, 256−264.
(77) Knowles, P. J.; Andrews, J. S.; Amos, R. D.; Handy, N. C.; Pople, J. A. Restricted Møller—Plesset theory for open-shell molecules. *Chem. Phys. Lett.* **1991**, *186*, 130−136.
(78) Knowles, P. J.; Werner, H.-J. Internally contracted multi-configuration-reference configuration interaction calculations for excited states. *Theor. Chim. Acta.* **1992**, *84*, 95−103.
(79) Knowles, P.; Handy, N. Determinant based full configuration interaction program.[FCI]. *Comput. Phys. Commun.;(Netherlands)* **1989**, *54*, 75.
(80) Allen, W. et al. *INTDER 2005*; 2005. INTDER is a general program written by W. D. Allen and coworkers, which performs vibrational analysis and higher-order nonlinear transformations.
(81) Gaw, J. F.; Willets, A.; Green, W. H.; Handy, N. C. In *Advances in Molecular Vibrations and Collision Dynamics*; Bowman, J. M., Ratner, M. A., Eds.; JAI Press, Inc.: Greenwich, CT, 1991; pp 170−185.
(82) Watson, J. K. G. *Vibrational Spectra and Structure*; Elsevier: Amsterdam, 1977; Vol. *1*, pp 1−89.
(83) Lowdin, P.-O. *Advances in quantum chemistry*; Academic Press: 1979.
(84) Dübal, H.-R.; Quack, M. Tridiagonal Fermi resonance structure in the IR spectrum of the excited CH chromophore in CF_3H. *J. Chem. Phys.* **1984**, *81*, 3779−3791.
(85) Yu, Q.; Bowman, J. M.; Fortenberry, R. C.; Mancini, J. S.; Lee, T. J.; Crawford, T. D.; Klemperer, W.; Francisco, J. S. Structure, anharmonic vibrational frequencies, and intensities of $NNHNN^+$. *J. Chem. Phys.* **2015**, *119*, 11623−11631.
(86) Finney, B.; Fortenberry, R. C.; Francisco, J. S.; Peterson, K. A. A spectroscopic case for SPSi detection: The third-row in a single molecule. *J. Chem. Phys.* **2016**, *145*, 124311.
(87) Werner, H.-J.; Reinsch, E.-A. The self-consistent electron pairs method for multiconfiguration reference state functions. *J. Chem. Phys.* **1982**, *76*, 3144−3156.
(88) Werner, H.-J.; Knowles, P. J. An efficient internally contracted multiconfiguration-reference configuration interaction method. *J. Chem. Phys.* **1988**, *89*, 5803−5814.
(89) Knowles, P. J.; Werner, H.-J. An efficient method for the evaluation of coupling coefficients in configuration interaction calculations. *Chem. Phys. Lett.* **1988**, *145*, 514−522.
(90) Bartlett, R. J.; Park, Y. C.; Bauman, N. P.; Melnichuk, A.; Ranasinghe, D.; Ravi, M.; Perera, A. Index of multi-determinantal and multi-reference character in coupled-cluster theory. *J. Chem. Phys.* **2020**, *153*, 234103.
(91) Jiang, W.; DeYonker, N. J.; Wilson, A. K. Multireference character for 3d transition-metal-containing molecules. *J. Chem. Theory Comput.* **2012**, *8*, 460−468.
(92) Bassett, M. K.; Fortenberry, R. C. Symmetry breaking and spectral considerations of the surprisingly floppy c-C_3H^- radical and the related dipole-bound excited state of c-C_3H^-. *J. Chem. Phys.* **2017**, *146*, 224303.
(93) Martin, J. M.; Lee, T. J.; Taylor, P. R.; François, J.-P. The anharmonic force field of ethylene, C_2H_4, by means of accurate *ab initio* calculations. *J. Chem. Phys.* **1995**, *103*, 2589−2602.
(94) Martin, J. M.; Taylor, P. R. Accurate *ab initio* quartic force field for trans-HNNH and treatment of resonance polyads. *Spectrochim. Acta, Part A* **1997**, *53*, 1039−1050.
(95) Fortenberry, R. C.; Huang, X.; Francisco, J. S.; Crawford, T. D.; Lee, T. J. Quartic force field predictions of the fundamental vibrational frequencies and spectroscopic constants of the cations $HOCO^+$ and $DOCO^+$. *J. Chem. Phys.* **2012**, *136*, 234309.
(96) Jutier, L.; Léonard, C.; Gatti, F. Renner−Teller effect in linear tetra-atomic molecules. II. Rovibronic levels analysis of the $X^2\Pi_u$ electronic state of $HCCH^+$. *J. Chem. Phys.* **2009**, *130*, 134302.
(97) Perić, M.; Jerosimić, S.; Mitić, M.; Milovanović, M.; Ranković, R. Underlying theory of a model for the Renner−Teller effect in tetra-atomic molecules: $X^2\Pi_u$ electronic state of $C_2H_2^+$. *J. Chem. Phys.* **2015**, *142*, 174306.
(98) Perić, M.; Jerosimić, S.; Ranković, R.; Krmar, M.; Radić-Perić, J. An ab initio model for handling the Renner−Teller effect in tetra-atomic molecules. I. Introduction of coordinates and the Hamiltonian. *Chem. Phys.* **2006**, *330*, 60−72.
(99) Brown, J. The effective Hamiltonian for the Renner−Teller effect. *J. Mol. Spectrosc.* **1977**, *68*, 412−422.
(100) Gardner, M. B.; Westbrook, B. R.; Fortenberry, R. C.; Lee, T. J. Highly-Accurate Quartic Force Fields for the Prediction of Anharmonic Rotational Constants and Fundamental Vibrational Frequencies. *Spectrochim. Acta, Part A* **2021**, *248*, 119184.

https://doi.org/10.1021/acs.jpca.2c01340
J. Phys. Chem. A 2022, 126, 4132−4146